Hindawi
International Transactions on Electrical Energy Systems
Volume 2023, Article ID 5544267, 23 pages
https://doi.org/10.1155/2023/5544267

Research Article

Optimal Operation of Hydrogen Energy Coupling Integrated Energy System considering Green Certificate, Ladder-Type Carbon Joint Trading, and Dual-Incentive Demand Response

Jingying Yang,[1] **Xiu Ji**,[2] **Meng Li**,[2] **Dexin Li**,[1] **Meiyue Li**,[2] **Huanhuan Han**,[2] **and Jiqing Yu**[3]

[1]*State Grid Jilin Electric Power Co., Ltd., Electric Power Science Research Institute, Changchun 130000, China*
[2]*National Local Joint Engineering Research Center for Smart Distribution Grid Measurement and Control with Safety Operation Technology, Changchun Institute of Technology, Changchun 130000, China*
[3]*Jilin Electric Power Co., Ltd., Changchun 130000, China*

Correspondence should be addressed to Xiu Ji; jixiu523@ccit.edu.cn

Received 23 August 2023; Revised 1 December 2023; Accepted 12 December 2023; Published 29 December 2023

Academic Editor: Shaofeng Lu

Under the "carbon peak and carbon neutrality" goal, the construction of an efficient, low-carbon, and economical energy supply system is of great significance for advancing a dual carbon strategy. In allusion to the integrated energy systems (IES) with hydrogen energy coupling, a hydrogen energy coupling IES low-carbon optimization operation strategy that took account of green certificate and ladder-type carbon joint trading and dual-incentive demand response was proposed in this paper. First, a hydrogen energy multiuse system composed of an electrolyzer, a hydrogen fuel cell, a methane reactor, and hydrogen energy storage was constructed to make full use of the low-carbon cleaning characteristics of hydrogen energy. Besides, a combined model of hydrogen mixed with natural gas was established to improve the utilization efficiency of hydrogen energy. Second, a dual-incentive demand response model including price incentives and subsidy incentives was constructed to fully use the ability to adjust demand-side resources. Next, in view of the carbon emission reduction mechanism of the green certificate, a green certificate and ladder-type carbon joint trading mechanism was constructed. In addition, a green certificate trading mechanism and a reward and punishment tiered carbon trading mechanism had been introduced separately in the IES optimization operation model to reduce carbon emissions of the system. The calculation simulation sets up different scenarios for comparative analysis. As shown by the results, the proposed model could effectively improve renewable energy consumption capacity and energy utilization efficiency. The effectiveness of hydrogen energy utilization, demand respond, and green certification carbon trading mechanism in improving system economy and low-carbon efficiency is verified.

1. Introduction

In order to achieve the goal of "carbon peaking and carbon neutrality" and alleviate the contradiction between supply and demand, vigorously developing a hydrogen energy-centered energy supply system is one of the key ways to improve environmental pollution and promote the green and low-carbon transformation of the energy system [1, 2]. As a secondary green energy with zero pollution and zero emissions, hydrogen energy is of great significance to improve the operational flexibility and energy utilization efficiency of IES by coupling and optimizing hydrogen energy with other IES energy sources [3].

At present, most of the research on the application of hydrogen energy in IES mainly focuses on hydrogen energy storage, electricity-hydrogen production technology, hydrogen fuel cells, and related equipment involved in hydrogen production. The wind power-hydrogen production technology can effectively solve the current large-scale wind curtailment problem and is one of the important measures in IES to improve the wind power consumption capacity. Literature [4] described the characteristics of wind power-

hydrogen production, which laid the foundation for the exploration of electricity-hydrogen production technology. Literature [5] considered the synergistic relationship between hydrogen energy, photovoltaic power, and wind power and proposed an island IES autonomous system containing hydrogen energy. Literature [6] focused on the application of wind power-hydrogen production equipment in IES and discussed the different control methods of wind power-hydrogen production equipment. Through the mutual transformation and coupling of multiple energy sources, users' demand for multiple loads of electricity, heat, and hydrogen can be met at the same time. The above literature mainly takes advantage of the surplus wind power at night to produce hydrogen, but there is insufficient research on the utilization of hydrogen energy. Literature [7] established a refined model of P2G equipment, considered the operating characteristics of methane reactor and electrolyzer, and analyzed the two-stage operation mode of P2G equipment in detail. Literature [8] refined the power-to-gas process into three procedures: electricity-to-hydrogen, hydrogen-to-methane, and hydrogen-to-hydroelectricity, and simultaneously ladder-type carbon trading costs and hydrogen energy utilization were introduced into the IES optimization model, further realizing the consumption of wind power. However, most of the relevant research on the application of hydrogen energy in IES focuses on analyzing the energy flow characteristics of hydrogen energy coupling, and seldom considers the influence of demand-side energy consumption characteristics on the optimal operation of hydrogen energy IES. In addition, most of the existing research focuses on one or two hydrogen usage scenarios and does not involve the full-process and diversified utilization of hydrogen energy such as hydrogen production, hydrogen use, hydrogen-mixed gas, and hydrogen storage. Therefore, it is impossible to further exert the effective and clean characteristics of hydrogen energy.

With the strengthening of multiload coupling characteristics such as electricity, heat, cold, and gas, the traditional demand response has gradually evolved into integrated demand response (IDR). As an important controllable resource in IES operation, IDR can promote energy economic operation and smooth load curve [9]. Literature [10] proposed an electricity and gas energy hub framework considering IDR, which effectively balances the supply and demand relationship between natural gas and electricity. Literature [11] introduced a transferable and reducible load model and then proposed an IES economic scheduling model based on flexible loads. Literature [12] proposed an IES optimal scheduling model that takes into account the electricity, gas, and heat IDR by combining the coupling characteristics of electricity, heat, and gas loads. Literature [13] established an electricity-heat IES economic scheduling model considering incentive-type IDR and conditional risk and verified the effectiveness of IDR resources in improving energy utilization efficiency. Literature [14] established an electricity-heat IDR model including transferable and reducible loads and proposed an IES low-carbon optimization model that takes into account the flexible loads of electricity and heat and hydrogen energy utilization using hydrogen as the energy conversion medium. The above literature fully invokes the role of demand-side resources in improving the economic and energy utilization efficiency of IES and relieves the pressure of system energy supply and improves the consumption of renewable energy through flexible adjustment of loads, which is very important for the realization of economic and flexible operation of IES. However, the types of demand response resources considered in existing studies are relatively single, and there is lack of refined modeling of different types of IDR resources. Therefore, the response of demand-side resources has not been fully utilized.

In order to achieve the goal of "carbon peaking and carbon neutrality," two major trading policies, the carbon emission trading (CET) mechanism and the green certificate trading (GCT) mechanism, came into being. It plays an important role in reducing carbon emissions and promoting new energy consumption [15, 16]. The CET mechanism is one of the important means to guide the operation of the IES low-carbon economy [17]. Literature [18] introduced the CET mechanism into the IES economic optimization model, discussed the unit output before and after the introduction of the CET mechanism, and verified the effectiveness of the CET mechanism in reducing IES carbon emissions. Literature [19] improved the CET mechanism, segmented the unit carbon trading price according to the range of carbon emissions to propose a ladder-type carbon trading price, and then carried out the optimization of IES scheduling to achieve the minimum sum of the ladder-type carbon trading cost and operating cost. Based on the ladder-type CET mechanism, literature [20] proposed an IES low-carbon optimal scheduling strategy from the perspective of source-side centralized scheduling and analyzed the impact of carbon emission range, unit carbon trading price, and different scheduling models on IES optimization. As the penetration rate of a high proportion of renewable energy continues to increase, increasing the consumption of renewable energy is an important way to reduce carbon emissions. The GCT mechanism provides favorable policy support for improving the capacity of renewable energy consumption [21–23]. Literature [24] established a bilateral transaction model between power distributors and renewable energy generators based on Co-operative Game Theory and GCT mechanism, which improves the capacity of renewable energy consumption. Literature [25] allocated the green certificate quota according to the entropy weight method and constructed the provincial day-ahead electricity market clearing model and the international green certificate trading market clearing model, respectively. Based on the GCT mechanism, literature [26] proposed an IES operation optimization model considering the weight of renewable energy consumption responsibility, which improves the proportion of green electricity and system economy. The above literature only considers the influence of CET mechanism or GCT mechanism on the optimal operation of IES alone but does not study the influence of CET and GCT on the optimal operation of IES at the same time. Therefore, it cannot give full play to the low-carbon operation characteristics of IES to a greater extent.

In response to the above problems, this paper proposed a hydrogen energy coupled IES optimal scheduling model that takes into account green certificate-ladder joint carbon trading and multitype demand response. Table 1 shows the comparison between the framework proposed in this article and in existing literature:

(1) In view of the problem that existing research focuses on a relatively single hydrogen usage scenario, this paper constructs a diversified hydrogen energy utilization model that covers the entire process of hydrogen production, hydrogen use, hydrogen-mixed gas, and hydrogen storage. It establishes electrolyzers, hydrogen fuel power plants, methane reactor, and a model of hydrogen-mixed gas and combined heat and cold, enriching hydrogen energy utilization scenarios and further improving the energy utilization efficiency of IES.

(2) In order to give full play to the adjustment ability of demand-side resources, alternative flexible loads are introduced into the traditional demand response model, and a multitype demand response model including price-type, incentive-type, and substitution-type is constructed. Among them, real-time price strategy is used instead of time-of-use price strategy, and a price-type demand response model based on real-time price is constructed. The incentive-type demand response model uses ladder-type subsidy incentives, which can further encourage users to adjust their energy consumption strategies.

(3) A green certificate trading mechanism and a reward and punishment ladder-type carbon trading mechanism are constructed, respectively. This paper discusses the carbon emission reduction mechanism of green certificates and proposes a green certificate and ladder-type carbon joint trading mechanism. By combining the green certificate trading mechanism and the ladder-type carbon trading mechanism, it increases the consumption level of renewable energy and reduces carbon emissions.

2. Electricity-Heat-Cold-Gas-Hydrogen IES Equipment Model

The structure diagram of the electricity-heat/cold-gas-hydrogen IES system constructed in this paper is shown in Figure 1, including three parts: energy supply, energy hub, and energy demand. The equipment mainly includes a electrolytic (EL), a hydrogen energy coupling system consisting of methane reactor (MR) and hydrogen fuel cell (HFC), a cold-heat electric power supply system consisting of a gas boiler (GB), co-generation power (CHP) model, an air conditioner (AC), and an absorption refrigerator (AR), as well as a multisource energy storage system consisting of battery (BT), cold storage tank (CST), heat storage tank (HST), gas storage tank (GST), and hydrogen storage tank (HES). In addition, it also includes two types of renewable energy units: wind turbine (WT) and photovoltaic (PV).

2.1. Multiple Utilization of Hydrogen Energy. IES utilizes the coupling and complementary between hydrogen energy and electric, heat, cold, and gas energy to further enhance the flexibility of IES. Utilizing the high-efficiency and low-carbon characteristics of hydrogen energy can promote the transformation of energy supply to high-efficiency, clean and flexible, and realize the low-carbon economic operation of IES. The multiple utilization of hydrogen energy proposed in this paper is shown in Figure 2, including five procedures of hydrogen to electricity, hydrogen to heat and electricity, hydrogen to methane, hydrogen energy storage, and hydrogen-mixed combined heat and power.

2.1.1. Hydrogen Production. EL can realize the electric-hydrogen coupling by converting electric energy into hydrogen energy. A part of the hydrogen is directly converted into electricity and heat by the hydrogen fuel cell, and the other part is converted into natural gas through the methane reactor. The input-output conversion model of EL is as follows:

$$\begin{cases} P^{t}_{\mathrm{EL},H_2} = \eta_{\mathrm{EC}} P^{t}_{\mathrm{EL},e}, \\ P^{\min}_{\mathrm{EL},e} \le P_{\mathrm{EL},e}(t) \le P^{\max}_{\mathrm{EL},e}, \\ P^{\mathrm{down}}_{\mathrm{EL},e} \le P_{\mathrm{EL},e}(t+1) - P_{\mathrm{EL},e}(t) \le P^{\mathrm{up}}_{\mathrm{EL},e}, \end{cases} \tag{1}$$

where $P_{\mathrm{EL},H_2}(t)$ is the hydrogen production power of EL; η_{EL} is the hydrogen production efficiency of EL; $P_{\mathrm{EL},e}(t)$ is the electric power of EL; $P^{\mathrm{down}}_{\mathrm{EL},e}$ and $P^{\mathrm{up}}_{\mathrm{EL},e}$ are the minimum and maximum value of EL electric power ramp rate; and $P^{\min}_{\mathrm{EL},e}$ and $P^{\max}_{\mathrm{EL},e}$ are the minimum and maximum value of EL electric power.

2.1.2. Hydrogen to Heat and Electricity. HFC can realize the coupling between hydrogen energy and heat and electric energy and is an important coupling device in electricity-heat-cold-gas-hydrogen IES. Literature [27] showed that the electricity and heat conversion efficiency of HFC can be approximately regarded as a constant, so the model of HFC can be expressed as follows:

$$\begin{cases} P_{\mathrm{HFC},e}(t) = \eta^{e}_{\mathrm{HFC}} P_{\mathrm{HFC},H_2}(t), \\ H_{\mathrm{HFC},h}(t) = \eta^{h}_{\mathrm{HFC}} P_{\mathrm{HFC},H_2}(t), \\ P^{\min}_{\mathrm{HFC},H_2} \le P_{\mathrm{HFC},H_2}(t) \le P^{\max}_{\mathrm{HFC},H_2}, \\ P^{\mathrm{down}}_{\mathrm{HFC},H_2} \le P_{\mathrm{HFC},H_2}(t+1) - P_{\mathrm{HFC},H_2}(t) \le P^{\mathrm{up}}_{\mathrm{HFC},H_2}, \end{cases} \tag{2}$$

where $P_{\mathrm{HFC},H_2}(t)$ is the hydrogen power input to the HFC; η^{e}_{HFC} and η^{h}_{HFC} are, respectively, the electric and heat power conversion efficiencies of HFC; $P^{\mathrm{up}}_{\mathrm{HFC},H_2}$ and $P^{\mathrm{down}}_{\mathrm{HFC},H_2}$ are, respectively, the maximum and minimum value of HFC input hydrogen power ramp rate; $P_{\mathrm{HFC},e}(t)$ and $H_{\mathrm{HFC},h}(t)$ are, respectively, the electricity and heat production power of HFC; and $P^{\max}_{\mathrm{HFC},H_2}$ and $P^{\min}_{\mathrm{HFC},H_2}$ are the maximum and minimum values of HFC input hydrogen power, respectively.

Table 1: Taxonomy table comparing the relevant references.

Reference	Hydrogen energy utilization	Gas mixing with hydrogen	IDR	Carbon trading mechanism	Green certificate trading mechanism
4–7	√	×	×	×	×
8	√	√	×	√	×
10	×	×	√	×	×
11	×	×	√	×	×
12	×	×	√	√	×
13	×	×	√	√	×
14	√	×	√	√	×
18–20	×	×	×	√	×
24–26	×	×	×	×	√
Model in this article	√	√	√	√	√

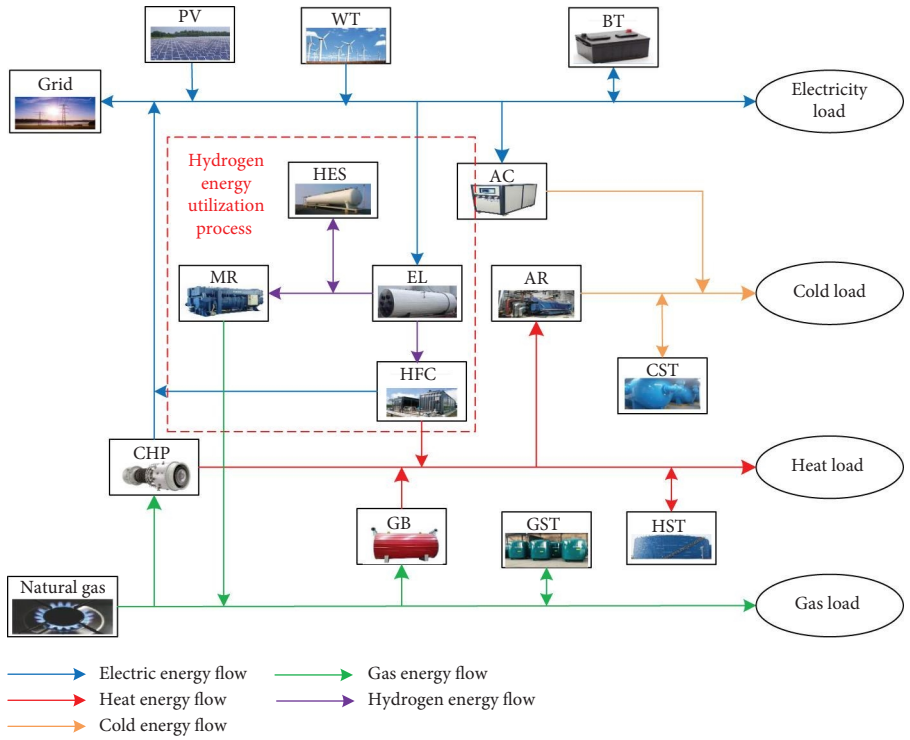

Figure 1: Structure diagram of electricity-heat-cold-gas hydrogen coupling IES.

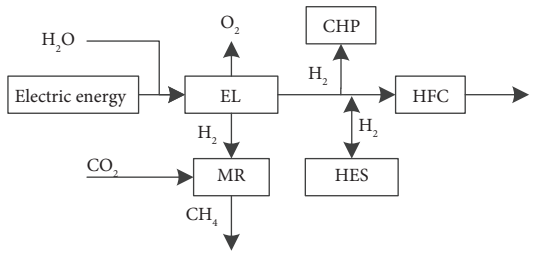

Figure 2: Multiple utilization of hydrogen energy.

2.1.3. Hydrogen to Methane. MR can use the hydrogen produced by the electrolyzer to realize hydrogen methanation and inject it into the natural gas pipeline of IES to provide gas energy. The input-output model of MR can be expressed as follows:

$$\begin{cases} P_{\mathrm{MR},g}(t) = \eta_{\mathrm{MR}} P_{\mathrm{MR},H_2}(t), \\ P^{\min}_{\mathrm{MR},H_2} \le P_{\mathrm{MR},H_2}(t) \le P^{\max}_{\mathrm{MR},H_2}, \\ P^{\mathrm{down}}_{\mathrm{MR},H_2} \le P_{\mathrm{MR},H_2}(t+1) - P_{\mathrm{MR},H_2}(t) \le P^{\mathrm{up}}_{\mathrm{MR},H_2}, \end{cases} \tag{3}$$

where η_{MR} is the methanation efficiency of MR; $P_{\mathrm{MR},H_2}(t)$ and $P_{\mathrm{MR},g}(t)$ are the hydrogen power input to MR and the gas power output to MR; and $P^{\max}_{\mathrm{MR},H_2}/P^{\min}_{\mathrm{MR},H_2}$ and $P^{\mathrm{up}}_{\mathrm{MR},H_2}/P^{\mathrm{down}}_{\mathrm{MR},H_2}$ are the upper/lower limit of hydrogen power input to MR and the upper/lower limit of ramp rate input to MR, respectively.

2.1.4. Hydrogen Storage. How to store hydrogen safely and efficiently has always been a major problem in the large-scale application of hydrogen energy. As China increases its support for the development of hydrogen energy, the

development progress of hydrogen storage is also accelerating. At present, high-pressure gaseous hydrogen storage technology is the most mature storage and transportation technology. It stores hydrogen in a gas tank in a high-density gaseous form through a compressor and releases hydrogen directly through a pressure reducing valve when used. With the characteristics of low cost, low energy consumption, and easy dehydrogenation, this device is widely used in various fields. This article stores hydrogen with high-pressure gaseous hydrogen storage technology, and its mathematical model is as follows:

$$\begin{cases} S_{\text{Tank}}^{t} = S_{\text{Tank}}^{t-1} + \left(v_{\text{in},H}^{t} - v_{\text{out},H}^{t}\right) \cdot \Delta t, \\ P_{\text{HES,chr}}^{t} = v_{\text{in},H}^{t} V_{H_2}, \\ P_{\text{HES,dis}}^{t} = v_{\text{out},H}^{t} V_{H_2}, \\ P_{\text{Tank}}^{t} = \dfrac{\rho_{H_2} S_{\text{Tank}}^{t} m_{\text{mol}} T_{\text{Tank}}}{R_{H_2} V_{\text{Tank}}}, \\ S_{\text{HES}}^{t} = \dfrac{P_{\text{Tank}}^{t}}{P_{\max}}, \\ P_{\text{HES,chr}}^{\min} \le P_{\text{HES,chr}}^{t} \le P_{\text{HES,chr}}^{\max}, \\ P_{\text{HES,dis}}^{\min} \le P_{\text{HES,dis}}^{t} \le P_{\text{HES,dis}}^{\max}, \end{cases} \tag{4}$$

where P_{Tank}^{t} and $P_{\max}$ are the pressure in the HES tank and its upper limit value, respectively; S_{Tank}^{t} is the hydrogen storage capacity of HES; ρ_{H_2} and R_{H_2} are the density and relative molecular mass of hydrogen, respectively; m_{mol} is the molar gas constant; T_{Tank} is the gas temperatures in the HES tank; $v_{\text{in},H}^{t}$ and $v_{\text{out},H}^{t}$ are the hydrogen charging speed and hydrogen releasing speed of HES, respectively; $P_{\text{HES,chr}}^{t}$ and $P_{\text{HES,dis}}^{t}$ are the hydrogen charging power and hydrogen releasing power, respectively; V_{Tank} is the tank volume of HES; S_{HES}^{t} is the hydrogen storage status of HES; and $P_{\text{hes},c}^{\max}$ and $P_{\text{hes},d}^{\max}$ are the maximum values of hydrogen charging power and hydrogen releasing power, respectively.

2.2. Combined Cold, Heat, and Power

2.2.1. Hydrogen-Mixed Combined Heat and Power Model. Based on literature [27], controlling the volume of hydrogen mixed with natural gas within 20% can effectively reduce the cost of gas energy purchase and carbon emissions. Therefore, in order to further improve the utilization and efficiency of hydrogen energy, a hydrogen-mixed CHP model is constructed. The total amount of natural gas mixed with hydrogen after introducing the hydrogen can be expressed as follows:

$$P_{\text{CHP}}(t) = \alpha_{\text{mix}}\left(\frac{P_{\text{CHP},H_2}(t)}{L_{H_2}} + \frac{P_{\text{CHP,Gas}}(t)}{L_{\text{Gas}}}\right), \tag{5}$$

$$\alpha_{\text{mix}} = \lambda(t) L_{H_2} + [1 - \lambda(t)] L_{\text{CH}_2}, \tag{6}$$

where $P_{\text{CHP}}(t)$ is the total amount of natural gas mixed with hydrogen input to CHP; $P_{\text{CHP},H_2}(t)$ is the amount of hydrogen input to CHP; L_{H_2} is the low calorific value of hydrogen; $P_{\text{CHP,Gas}}(t)$ is the amount of natural gas input to CHP; L_{Gas} is the the low calorific value of natural gas; α_{mix} is the low calorific value of natural gas mixed with hydrogen; and $\lambda(t)$ is the ratio of gas mixed with hydrogen.

The gas-hydrogen mixing ratio $\lambda(t)$ in period t can be expressed as follows:

$$\lambda(t) = \frac{P_{\text{CHP},H_2}(t)/L_{H_2}}{P_{\text{CHP},H_2}(t)/L_{H_2} + P_{\text{CHP,Gas}}(t)/L_{\text{Gas}}}, \tag{7}$$

$$0 \le \lambda(t) \le 20\%. \tag{8}$$

Therefore, the hydrogen-mixed CHP model can be expressed as follows:

$$\begin{cases} P_{\text{CHP},e}(t) = \eta_{\text{CHP},e} P_{\text{CHP}}(t), \\ P_{\text{CHP},h}(t) = \eta_{\text{CHP},h} P_{\text{CHP}}(t), \end{cases} \tag{9}$$

where $\eta_{\text{CHP},e}$ and $\eta_{\text{CHP},h}$ are the electric and heat power conversion efficiencies of the hydrogen-mixed CHP, respectively; $P_{\text{CHP},e}(t)$ and $P_{\text{CHP},h}(t)$ are the electric and heat powers of the hydrogen-mixed CHP, respectively.

2.2.2. Gas Boiler. GB uses natural gas as fuel for heating. The heat produced by GB is efficient and environmentally friendly, and its heat production efficiency is also high. The relationship between the output heat power and the input gas power of GB is as follows:

$$\begin{cases} P_{\text{GB},h}(t) = \eta_{\text{GB}} P_{\text{GB},g}(t), \\ 0 \le P_{\text{GB},h}(t) \le P_{\text{GB},h}^{\max}, \end{cases} \tag{10}$$

where $P_{\text{GB},h}(t)$ is the heat power output by GB; $P_{\text{GB},g}(t)$ is the amount of natural gas consumed by GB; $P_{\text{GB},h}^{\max}$ is the upper limit of heat power output by GB; and η_{GB} is the heat efficiency of GB.

2.2.3. Air Conditioning. AC meets the cooling needs of users by converting electric energy into cold energy. The relationship between AC input electric power and output cold energy is as follows:

$$\begin{cases} P_{\text{AC},c}(t) = \eta_{\text{AC}} P_{\text{AC},e}(t), \\ 0 \le P_{\text{AC},e}(t) \le P_{\text{AC},e}^{\max}, \end{cases} \tag{11}$$

where $P_{\text{AC},c}(t)$ is the cold energy output by AC; η_{AC} is the cooling coefficient of AC; $P_{\text{AC},e}(t)$ is the electric power input to AC; and $P_{\text{AC},e}^{\max}$ is the upper limit of electric power of AC.

2.2.4. Absorption Refrigerator. AR can use the recovered waste heat for refrigeration. It mainly uses high-temperature liquid refrigerant to reduce the pressure and then refrigerates through low-temperature and low-pressure gasification. The model is as follows:

$$\begin{cases} P_{\mathrm{AR},c}(t) = \eta_{\mathrm{AR}} P_{\mathrm{AR},h}(t), \\ 0 \le P_{\mathrm{AR},h}(t) \le P_{\mathrm{AR},h}^{\max}, \end{cases} \tag{12}$$

where $P_{\mathrm{AR},c}(t)$ is the cold energy output by AR; η_{AR} is the refrigeration coefficient of AR; $P_{\mathrm{AR},h}(t)$ is the heat consumed by AR; and $Q_{\mathrm{AR}}^{\max}$ is the upper limit of heat power of AR.

2.3. Multisource Energy Storage. Energy storage equipment can realize the transfer of energy in the time dimension to improve energy utilization and reduce energy costs. Commonly used energy storage devices in IES include batteries, heat storage tanks, gas storage tanks, and cold storage tanks. Their energy charging and discharging processes are similar, and the limitations of charging and discharging power and storage capacity must be considered. The difference is that electric energy is fast and flexible, but its storage costs are high, while heat/cold energy and natural gas are easy to store and have a slower response time. Based on literature [28], similar constraint models can be used for batteries, heat storage tanks, gas storage tanks, and cold storage tanks, which can be expressed as follows.

2.3.1. Energy Storage Capacity Constraints. Considering the energy loss and efficiency of charging and discharging, the energy storage capacity of energy storage device x and its constraints shall satisfy the following formulas:

$$\begin{cases} S_x(t) = S_x(t-1)(1-\gamma_x) + \left(P_{x,\mathrm{chr}}(t)\eta_{x,\mathrm{chr}} - \dfrac{P_{x,\mathrm{dis}}(t)}{\eta_{x,\mathrm{dis}}} \right)\Delta t, \\ S_x^{\min} \le S_x(t) \le S_x^{\max}, \\ S_x(24) = S_x(0), \end{cases} \tag{13}$$

where $x \in \{\mathrm{BT}, \mathrm{HST}, \mathrm{GST}, \mathrm{CST}\}$, $\eta_{x,\mathrm{chr}}$ and $\eta_{x,\mathrm{dis}}$ are the charging and discharging efficiencies of the energy storage device x, respectively; $S_x^{\min}$ and $S_x^{\max}$ are the minimum and maximum value of the energy storage capacity S_x^t of the energy storage device x; $S_x(24)$ and $S_x(0)$ are, respectively, energy storage capacity at the beginning and end of a day scheduling cycle; and γ_x is the energy self-loss rate of energy storage device x.

2.3.2. Charge and Discharge State Constraints. The charging and discharging states of energy storage device x need to satisfy mutually exclusive constraints. In addition, in order to prevent the aging of BT, BT also needs to meet the charge and discharge frequency constraints:

$$U_{x,\mathrm{chr}}(t) + U_{x,\mathrm{dis}}(t) \le 1, \tag{14}$$

where $U_{x,\mathrm{chr}}(t)$ and $U_{x,\mathrm{dis}}(t)$ are, respectively, the charging and discharging state flags of the energy storage device x, 0 means outage and 1 means running; $U_{\mathrm{BT,dis}}(t)$ and $U_{\mathrm{BT,chr}}(t)$ are, respectively, the charging and discharging status mark bits of BT; and T_{BT} is the total charging and discharging frequency of BT.

2.3.3. Output Constraint and Ramp Rate Constraint. Considering the life-span factor, the energy storage device must meet the upper and lower limits of the charge and discharge power and the upper and lower limits of the ramp rate:

$$\begin{cases} U_{x,\mathrm{chr}}(t) P_{x,\mathrm{chr}}^{\min} \le P_{x,\mathrm{chr}}(t) \le U_{x,\mathrm{chr}}(t) P_{x,\mathrm{chr}}^{\max}, \\ U_{x,\mathrm{dis}}(t) P_{x,\mathrm{dis}}^{\min} \le P_{x,\mathrm{dis}}(t) \le U_{x,\mathrm{dis}}(t) P_{x,\mathrm{dis}}^{\max}, \\ P_{x,\mathrm{chr}}^{\mathrm{down}} \le P_{x,\mathrm{chr}}(t) - P_{x,\mathrm{chr}}(t-1) \le P_{x,\mathrm{chr}}^{\mathrm{up}}, \\ P_{x,\mathrm{dis}}^{\mathrm{down}} \le P_{x,\mathrm{dis}}(t) - P_{x,\mathrm{dis}}(t-1) \le P_{x,\mathrm{dis}}^{\mathrm{up}}, \end{cases} \tag{15}$$

where $P_{x,\mathrm{chr}}(t)$ and $P_{x,\mathrm{dis}}(t)$ are the charging and discharging powers of the electricity storage and heating devices, respectively; $P_{x,\mathrm{chr}}^{\min}/P_{\mathrm{x,dis}}^{\min}$ and $P_{x,\mathrm{dis}}^{\max}/P_{x,\mathrm{chr}}^{\max}$ are the upper and lower limits of the charging/discharging power of the energy storage device x, respectively; and $P_{x,\mathrm{chr}}^{\mathrm{up}}/P_{x,\mathrm{dis}}^{\mathrm{up}}$ and $P_{x,\mathrm{chr}}^{\mathrm{down}}/P_{x,\mathrm{dis}}^{\mathrm{down}}$ are the upper and lower limits of the ramp rate of the charging/discharging power of the energy storage device x, respectively.

3. Green Certificate and Ladder-Type Carbon Joint Trading Mechanisms

3.1. Green Certificate Trading Mechanism. The quantity of green certificate is positively correlated with the amount of electricity generated by the renewable energy. The green certificate refers to the national certification of renewable energy grid electricity, and it is also a certificate for the consumption of green electricity on the demand side. Similar to the carbon trading mechanism, the green certificate trading mechanism also uses transactions to play the role of the market in the optimal allocation of resources. When the number of green certificates in the energy system exceeds the free green certificate quota of the system, the surplus green certificates can be sold in the green certificate trading market to obtain certain income. On the contrary, it is necessary to purchase green certificates from the market to meet the green certificate quota indicators. The calculation formula of green certificate trading cost can be expressed as follows:

$$\begin{cases} D_P = \delta_P \sum_{t=1}^{T} L_{\mathrm{e}}(t), \\ D_S = \varepsilon_{\mathrm{LZ}} \sum_{t=1}^{T} \left(P_{WT}(t) + P_{PV}(t) \right), \\ F_{\mathrm{GCT}} = c_{\mathrm{GCT}} \left(D_S - D_P \right), \end{cases} \tag{16}$$

where δ_P is the quota coefficient of the number of green certificates allocated in the IES; $\varepsilon_{\mathrm{LZ}}$ is the conversion coefficient of WT power generation into the number of green certificates, and 1 green certificate corresponds to the WT

settlement amount of 1 MWh; L_e^t is the actual power demand of the user; $P_{WT}(t)$ and $P_{PV}(t)$ are, respectively, the output electric power of WT and PV; D_P is the quota for the number of green certificates held by IES; D_S is the number of green certificates obtained for IES new energy power generation; c_{GCT} is the green certificate transaction price; and F_{GCT} is the green certificate transaction cost of IES.

In this paper, the Cournot transaction model based on quantity competition represents the green certificate trading price. According to the Cournot model formula, the green certificate trading price model can be expressed as follows:

$$c_{GCT} = \alpha'_{GCT} - \chi'_{GCT} D_c, \tag{17}$$

where α'_{GCT} and χ'_{GCT} are, respectively, two positive parameters of the inverse price function in the Cournot transaction model and D_c is the number of green certificates sold by IES.

Among them, α'_{GCT} and χ'_{GCT} are expressed as follows:

$$\begin{cases} \alpha'_{GCT} = c_{GCT,0}, \\ \chi'_{GCT} = \dfrac{(1-\varepsilon'_{GCT})c_{GCT,0}}{\delta_Q \sum_{t=1}^{T} L_e(t)}, \end{cases} \tag{18}$$

where $c_{GCT,0}$ is the basic transaction price of the green certificate and ε'_{GCT} is the GCT transaction price ratio calculated based on historical data.

Since China's green certificates are currently mainly oriented to users with renewable energy, their application in optimal scheduling of integrated energy systems is limited to theoretical research. Therefore, the authors make the following assumptions:

(1) The policy encourages the integrated energy system to participate in green certificate trading and allows the integrated energy system to generate the electricity for trading

(2) The trust mechanism should be established by government and both parties to the transaction to ensure the fairness and equity of green certificate trading

(3) Integrated energy system participating in green certificate trading has sufficient capacity to reduce carbon emissions and increase power output

(4) Rules and policies for green certificate trading are stable to avoid market fluctuations from adversely affecting the integrated energy system

It should be noted that these assumptions may require further verification and refinement in actual operations. At the same time, changes in policies and market environment may also affect the effectiveness of the integrated energy system participating in green certificate trading.

3.2. Carbon Trading Mechanism. The carbon trading mechanism refers to the free trading of CO_2 emission rights in order to control the carbon emissions of various energy sectors. The main equipment that emits CO_2 in the IES includes CHP units, GB, and outsourced electricity (here, it is considered that the outsourced electricity in IES comes from coal-fired power plants) [8], and their specific distribution is as follows:

$$E_{PE} = E_{GB} + E_{CHP} + E_{Grid}, \tag{19}$$

$$E_{GB} = \sum_{t=1}^{T} \delta_h P_{GB,h}(t), \tag{20}$$

$$E_{CHP} = \sum_{t=1}^{T} \delta_h \left(\lambda_{e-h} P_{CHP,e}(t) + P_{CHP,h}(t)\right), \tag{21}$$

$$E_{Grid} = \sum_{t=1}^{T} \delta_e P_{Grid}(t), \tag{22}$$

where T represents the scheduling cycle; E_{GB}, E_{CHP}, and E_{Grid} are the free carbon emission quotas allocated by GB, CHP, and external power purchases, respectively; λ_{e-h} is the electricity-heat conversion coefficient; E_{PE} is the total amount of IES carbon allowances; $P_{Grid}(t)$ is the outsourced electricity from external grid for IES; and δ_e and δ_h are carbon emission quotas for unit electricity and unit heat, respectively, which are 0.728t (MWh) and 0.102t (GJ) [29].

According to literature [29], the IES actual carbon emission model can be expressed as follows:

$$E_{Grid}^{act} = \sum_{t=1}^{T} \left(x_1 (P_{Grid}(t))^2 + y_1 P_{Grid}(t) + z_1\right), \tag{23}$$

$$\begin{cases} E_{total}^{act} = \sum_{t=1}^{T} \left(x_2 (P_{total}(t))^2 + y_2 P_{total}(t) + z_2\right), \\ P_{total}(t) = \lambda_{e-h} P_{CHP,e}(t) + P_{GB,h}(t) + P_{CHP,h}(t), \end{cases} \tag{24}$$

where x_1, y_1, and z_1 are the carbon emission calculation coefficients of coal-fired units; E_{Grid}^{act} is the actual carbon emissions of IES outsourced electricity; x_2, y_2, and z_2 are the carbon emission calculation coefficients of gas-fired units; E_{total}^{act} is the actual carbon emission of all the gas-fired units of IES; and $P_{total}(t)$ is the equivalent output power of GT, GB and WHB.

Considering that the methane reactor MR can absorb a part of carbon dioxide in the process of hydrogen energy conversion to natural gas, it is also necessary to consider the amount of carbon dioxide absorbed by MR. The amount of carbon dioxide absorbed by MR is expressed as follows:

$$E_{MR} = \sum_{t=1}^{T} \varphi_{MR} P_{MR,g}(t), \tag{25}$$

where E_{MR} is the amount of carbon dioxide absorbed by MR and φ_{MR} is the absorption efficiency of MR.

Therefore, E_{IES}^{act}, the total actual carbon emissions of IES, can be expressed as follows:

$$E_{IES}^{act} = E_{Grid}^{act} + E_{total}^{act} - E_{MR}. \tag{26}$$

The cost of traditional carbon trading is given by multiplying the difference between the actual carbon emissions and the carbon quota allocated free of charge by the carbon

trading price in the market. However, the carbon trading price is a fixed value, and its mathematical model is as follows:

$$F_{\mathrm{CET}} = c\left(E_{\mathrm{IES}}^{\mathrm{act}} - E_{\mathrm{PE}}\right), \tag{27}$$

where F_{CET} is the carbon trading cost borne by IES and c is the carbon trading price in the market.

3.3. Green Certificate-Carbon Trading Joint Mechanism. Since the carbon emission reduction of new energy supply can be obtained by calculation [22], the green certificate-carbon joint trading can be realized through the combination of the green certificate,carbon trading mechanism and the green certificate trading mechanism. Generally speaking, after considering the green certificate trading mechanism, when evaluating carbon emission rights, new energy can promote the reduction of carbon emissions, which affects the carbon trading mechanism. At this time, the green certificate can participate in the carbon trading mechanism and the green certificate trading mechanism at the same time and realize the joint interaction between the two parties through market guidance on factors such as transaction price and demand. The specific steps of the green certificate-carbon joint trading mechanism are as follows:

Step 1. Calculate the carbon emissions of the IES. Calculate the CO_2 emissions of IES coal-fired units and gas-fired units during use according to formulas (23) and (24).

Step 2. Analyze the carbon emission reduction of the green certificate. Due to the relatively high proportion of coal-fired power generation in China, this paper compares the CO_2 emission equivalents produced by coal-fired power generation and new energy power generation to obtain the carbon emission reduction behind the green certificate. The calculation formula is as follows [22]:

$$F_{\mathrm{green}} = E_{\mathrm{coal}} - E_{\mathrm{green}}, \tag{28}$$

where F_{green} is the carbon emission reduction embodied in new energy power generation and E_{green} and E_{coal} are the CO_2 emission equivalents of new energy power supply and coal-fired energy supply in the life cycle of their industrial chains, respectively.

Step 3. Calculate the CET cost of new energy offsetting carbon emissions. Based on formulas (19)–(27), since the new energy supply offsets a part of the carbon emissions, the actual carbon emissions of the IES can be rewritten as follows:

$$E_{\mathrm{IES}}^{\mathrm{act}} = E_{\mathrm{Grid}}^{\mathrm{act}} + E_{\mathrm{total}}^{\mathrm{act}} - E_{\mathrm{MR}} - D_P F_{\mathrm{green}}. \tag{29}$$

In order to further reduce the carbon emissions of IES, the carbon trading price is segmented to construct a ladder-type carbon trading price. In order to encourage the low-carbon development of enterprises, reward and punishment coefficients are introduced, and the carbon trading process is divided into two parts: reward and punishment. In order to further encourage enterprises to save energy and reduce emissions, the government provides certain technical subsidies to them, and the carbon transaction cost of this part can be expressed as follows:

$$F_{\mathrm{CET}}^{t} = \begin{cases} -c\,(1+2\varepsilon)\left(E_{\mathrm{PE}} - h - E_{\mathrm{IES}}^{\mathrm{act}}\right), & E_{\mathrm{IES}}^{\mathrm{act}} \le E_{\mathrm{PE}} - h, \\ -c\,(1+2\varepsilon)h - c\,(1+\varepsilon)\left(E_{\mathrm{PE}} - E_{\mathrm{IES}}^{\mathrm{act}}\right), & E_{\mathrm{PE}} - h \le E_{\mathrm{IES}}^{\mathrm{act}} \le E_{\mathrm{PE}}. \end{cases} \tag{30}$$

However, when the actual carbon emissions are greater than the free carbon allowances, it means that the energy sector needs to purchase excess carbon allowances in the carbon trading market, and the carbon trading cost is positive, which means that the IES needs to bear the carbon trading costs. The greater the IES carbon emissions, the greater the corresponding carbon trading price. The carbon trading cost of this part can be expressed as follows:

$$F_{\mathrm{CET}}^{t} = \begin{cases} c\left(E_{\mathrm{IES}}^{\mathrm{act}} - E_{\mathrm{PE}}\right), & E_{\mathrm{PE}} < E_{\mathrm{IES}}^{\mathrm{act}} < E_{\mathrm{PE}} + h, \\ \mathrm{ch} + c\,(1+\mu)\left(E_{\mathrm{IES}}^{\mathrm{act}} - E_{\mathrm{PE}} - h\right), & E_{\mathrm{PE}} + h < E_{\mathrm{IES}}^{\mathrm{act}} < E_{\mathrm{PE}} + 2h, \\ c\,(2+\mu)h + c\,(1+2\mu)\left(E_{\mathrm{IES}}^{\mathrm{act}} - E_{\mathrm{PE}} - 2h\right), & E_{\mathrm{PE}} + 2h < E_{\mathrm{IES}}^{\mathrm{act}} < E_{\mathrm{PE}} + 3h, \\ c\,(3+3\mu)h + c\,(1+3\mu)\left(E_{\mathrm{IES}}^{\mathrm{act}} - E_{\mathrm{PE}} - 3h\right), & E_{PE} + 3h < E_{\mathrm{IES}}^{\mathrm{act}}, \end{cases} \tag{31}$$

where c is the carbon transaction price in the market; $F_{\mathrm{co}_2}^{t}$ is the reward and punishment ladder carbon transaction cost borne by IES; h is the length of the carbon emission interval; and ε and μ are the reward coefficient and punishment coefficient, respectively.

According to the above model, the relationship between its carbon emissions and carbon trading price can be intuitively represented by Figure 3.

4. Multitype Demand Response Model

Traditional demand response is to adjust electricity consumption behavior based on electricity price signals or incentive policies to achieve the peak shaving and valley filling effect of electricity load. With the development of IES, the loads in users show a diversified trend. The IDR strategy can break the boundaries between different energy sources and

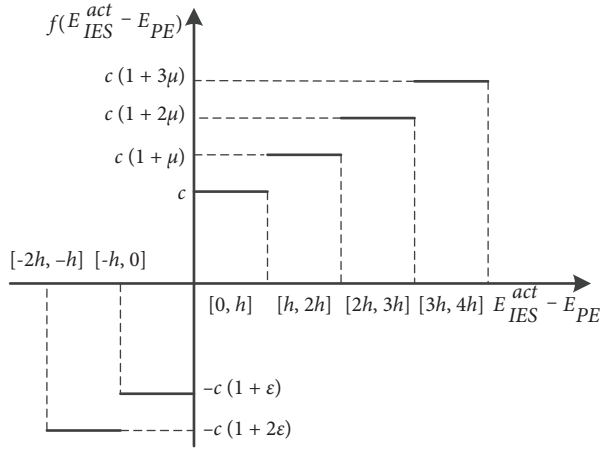

Figure 3: Relationship between carbon emissions and ladder-type carbon trading prices.

achieve time transfer and coupling complementation of multiple loads. In order to give full play to the response of IDR resources, this paper comprehensively considers three types of IDR models: price-type, incentive-type, and substitution-type, and constructs a multitype IDR model for electricity, heat, cold, and gas loads.

4.1. Price-Type IDR Model. Price-type IDR strategies are mainly divided into two categories, namely, time-of-use price strategy and real-time price strategy. Time-of-use electricity price is currently the most widely used price-type IDR pricing mechanism. However, the peak and valley periods of time-of-use electricity price are relatively fixed, and the energy price information is relatively single, which cannot reflect the changing needs of user loads in real time. As a derivative and improvement of time-of-use electricity price IDR, the price information update step of the real-time price IDR strategy is usually one hour, which can more accurately reflect the real-time relationship between supply and demand and dynamically guide users to participate in IDR. The time scale of real-time price strategy update is short, and it has high requirements on communication systems, infrastructure, and other conditions, but the accuracy of real-time prices is higher and more realistic. Based on the above, this chapter adopts the IDR model based on real-time price strategy.

The price demand elasticity matrix is used to describe the characteristics of transferable electricity and gas loads. First, assume that the element $e_i(t, j)$ in the row t and column j of the demand elasticity matrix $\mathbf{E}_i(t, j)$ be the elasticity coefficient of type i load at time t to the price at time j, which can be expressed as follows:

$$e_i(t, j) = \frac{\Delta L_{i,L}(t)/L_{i,0}(t)}{\Delta c_i(j)/c_{i,0}(j)}, \tag{32}$$

where $i \in \{e, g\}$; $\Delta L_{i,L}(t)$ is the change amount of type i load after IDR; $L_{i,0}(t)$ is the initial load amount of type i; $\Delta c_i(j)$ is the price change of type i energy after IDR in period j; $c_{i,0}(j)$ is the initial price of type i energy in period j. Therefore, the transferable electric and gas load changes after IDR can be expressed as follows:

$$\Delta L_{i,L}(t) = L_{i,0}(t)\left[\sum_{j=1}^{T} \mathbf{E}_i(t, j)\frac{c_i(j) - c_{i,0}(j)}{c_{i,0}(j)}\right], \tag{33}$$

where T represents the scheduling period and $c_i(j)$ is the energy price of type i.

Assume that the price update step is 1 hour and since the real-time price cannot fluctuate significantly, the real-time price needs to satisfy upper and lower constraints and fluctuation constraints, which can be expressed as follows:

$$\begin{cases} c_{i,b}(t) = \lambda_i(t)c_{i,0}(t), \lambda_i(t) = \dfrac{L_{i,0}(t)}{\left(\sum_{t=1}^{T} L_{i,0}(t)/T\right)}, \\ c_{i,\min}(t) \le c_i(t) \le c_{i,\max}(t), \\ \Delta c_{i,\min}(t) \le c_i(t) - c_{i,b}(t) \le \Delta c_{i,\max}(t), \\ 0 \le \left|\Delta L_{i,L}(t)\right| \le L_{i,L,\max}(t), \end{cases} \tag{34}$$

where $c_{i,b}^t$ is the energy price benchmark value; λ_i^t is the real-time benchmark price floating coefficient; $c_{i,\min}^t$ and $c_{e,\max}^t$ are the minimum and maximum values of the real-time energy price respectively; $\Delta c_{i,\min}^t$ and $\Delta c_{i,\max}^t$ are the minimum and maximum values of the real-time energy price fluctuation constraints, respectively; and $L_{i,L,\max}^t$ is the upper limit of change in the i type of transferable load.

4.2. Incentive-Type IDR Model

4.2.1. Incentive-Type Electric and Gas Load. Since the user's electric and gas loads are relatively fixed in a day, the peak period of electricity and gas consumption is usually the peak period of the user's life and production. At this time, if the electric load and gas load are reduced, the users' sense of satisfaction will be impacted. In addition, the purchase price of the electric load and gas load at the peak period is relatively high. Therefore, in order to minimize the impact on users' lives, an incentive subsidy mechanism based on time-of-use prices of electricity and gas is adopted for reducing the loads of electricity and gas [30].

$$\begin{aligned} E_{\mathrm{IDR},e}(t) &= \varepsilon_e c_e(t) L_{e,\mathrm{cut}}(t), \\ E_{\mathrm{IDR},e}(t) &= \varepsilon_e c_e(t) L_{e,\mathrm{cut}}(t), \end{aligned} \tag{35}$$

where ε_e and ε_g are, respectively, the reduction subsidy coefficients of electric load and gas load; $L_{e,\mathrm{cut}}(t)$ and $L_{g,\mathrm{cut}}(t)$ are, respectively, the amount of electricity load and gas load cut by users; and $E_{\mathrm{IDR},e}(t)$ and $E_{\mathrm{IDR},g}(t)$ are, respectively, the incentive subsidy costs for users to cut electricity load and gas load.

For the reduced electric load and gas load, the adjustments of electric load and gas load at time t should be within a certain range, and the total load change within 1 day should also meet the constraint, realizing the user's sense of comfort in energy consumption:

$$\begin{cases} L_{e,\mathrm{cut}}(t) \le \varphi_{e,\mathrm{cut}} L_{e,0}(t), \\ \sum_{t=1}^{T} L_{e,\mathrm{cut}}(t) \le \varphi_{\mathrm{total}}^{e} \sum_{t=1}^{T} L_{e,0}(t), \\ L_{g,\mathrm{cut}}(t) \le \varphi_{g,\mathrm{cut}} L_{g,0}(t), \\ \sum_{t=1}^{T} L_{g,\mathrm{cut}}(t) \le \varphi_{\mathrm{total}}^{g} \sum_{t=1}^{T} L_{g,0}(t), \end{cases} \tag{36}$$

where $L_{e,0}(t)$ and $L_{g,0}(t)$ are the initial electric load and initial gas load, respectively; $\varphi_{e,\mathrm{cut}}$ and $\varphi_{g,\mathrm{cut}}$ are the upper limit of the reduction rate of the electric load and the gas load, respectively; $\varphi_{\mathrm{total}}^{e}$ and $\varphi_{\mathrm{total}}^{g}$ are the upper limit of the total reduction rate of the electric load and gas load, respectively.

4.2.2. Incentive-Type Heat and Cold Loads Response Model. Considering the perceptual ambiguity and time delay of heat and cold loads, it is not appropriate to use price signals to motivate users to participate in load adjustment. As the main adjustment index of heat and cold loads, literature [31] expressed the quantitative relationship between the demand of heat and cold loads, and the temperature of indoor and outdoor is shown in formulas (3)–(15):

$$\begin{cases} L_h(t) = f\left(T_{h,\mathrm{in}}(t)\right) = 3.6\left[S\varepsilon\left(T_{h,\mathrm{in}}(t) - T_{h,\mathrm{out}}(t)\right) + \dfrac{\mathrm{CS}}{\Delta t}\left(T_{h,\mathrm{in}}(t) - T_{h,\mathrm{in}}(t-1)\right)\right], \\ L_c(t) = f\left(T_{c,\mathrm{in}}(t)\right) = 3.6\left[S\varepsilon\left(T_{c,\mathrm{in}}(t) - T_{c,\mathrm{out}}(t)\right) + \dfrac{\mathrm{CS}}{\Delta t}\left(T_{c,\mathrm{in}}(t) - T_{c,\mathrm{in}}(t-1)\right)\right], \end{cases} \tag{37}$$

where ε is the indoor heat loss under the temperature difference of the unit building area; S is the building indoor area; C is the specific heat capacity per unit building area; $T_{h,\mathrm{in}}(t)$ and $T_{h,\mathrm{out}}(t)$ are the indoor and outdoor temperatures of the heating system; and $T_{c,\mathrm{in}}(t)$ and $T_{c,\mathrm{out}}(t)$ are, respectively, the indoor and outdoor temperatures of the cooling system.

The mathematical model of heat and cold loads response can be expressed as follows:

$$\begin{cases} \Delta L_h(t) = f\left(T_{h,\mathrm{in}}(t)\right) - f\left(T_{h,\mathrm{in}}(t) - \Delta T_{h,\mathrm{in}}(t)\right), 0 \le \Delta L_h(t) \le \Delta L_{h,\max}, \\ T^{\min} \le T_{h,\mathrm{in}}(t) - \Delta T_{h,\mathrm{in}}(t) \le T^{\max}, \\ \Delta L_c(t) = f\left(T_{c,\mathrm{in}}(t)\right) - f\left(T_{c,\mathrm{in}}(t) - \Delta T_{c,\mathrm{in}}(t)\right), 0 \le \Delta L_c(t) \le \Delta L_{c,\max}, \\ T^{\min} \le T_{c,\mathrm{in}}(t) - \Delta T_{c,\mathrm{in}}(t) \le T^{\max}, \end{cases} \tag{38}$$

where $\Delta T_{h,\mathrm{in}}(t)$ and $\Delta T_{c,\mathrm{in}}(t)$ are, respectively, the outdoor temperature variation of the heat system and the cold system; $\Delta L_h(t)$ and $\Delta L_c(t)$ are, respectively, the variation of heat load and cold load of the user at time t; $\Delta L_{h,\max}$ and $\Delta L_{c,\max}$ are, respectively, the upper limit of the user's heat load and cold load variation; and $T^{\max}$ and $T^{\min}$ are, respectively, the upper and lower limits of the user's comfort range.

Due to the ambiguity of the user's comfort requirements for room temperature, the smaller the change in the heat/cold load, the smaller the impact on the user's comfort; on the contrary, the greater the change in the heat/cold load, the greater the impact. It can be seen that the change in heat/cold load is not linearly related to the impact on users' satisfaction. Therefore, IES adopts a ladder-type compensation method to provide incentive subsidies to users for changes in heat/cold loads. The heat/cold load compensation fee for users at time t is as follows:

$$\begin{aligned} E_{h,\mathrm{IDR}}(t) &= \varepsilon_{h,\mathrm{IDR}} \Delta L_h(t), \\ E_{c,\mathrm{IDR}}(t) &= \varepsilon_{c,\mathrm{IDR}} \Delta L_c(t), \end{aligned} \tag{39}$$

where $E_{h,\mathrm{IDR}}(t)$ and $E_{c,\mathrm{IDR}}(t)$ are, respectively, the incentive IDR subsidy costs for the heat load and cold load and $\varepsilon_{h,\mathrm{IDR}}$ and $\varepsilon_{c,\mathrm{IDR}}$ are, respectively, the subsidy coefficients for the heat load and cold load changes.

Taking the heat load as an example, this paper adopts a ladder-type subsidy coefficient as considering that the greater the degree of heat load deviation, the greater the energy experience of users. It represents that the subsidy

coefficient changes in steps according to the actual load deviation degree, and the deviation degree is positively correlated with the subsidy coefficient. It can be expressed as follows:

$$\varepsilon_{h,\mathrm{IDR}} = \begin{cases} \varepsilon_{h,\mathrm{IDR}}, & 0 < \left|\Delta L_h(t)\right| < \alpha_1, \\ \left(1+\lambda_{h,\mathrm{IDR}}\right)\varepsilon_{h,\mathrm{IDR}}, & \alpha_1 \le \left|\Delta L_h(t)\right| \le \alpha_2, \\ \left(1+2\lambda_{h,\mathrm{IDR}}\right)\varepsilon_{h,\mathrm{IDR}} & \left|\Delta L_h(t)\right| > \alpha_2, \end{cases} \tag{40}$$

where $\lambda_{h,\mathrm{IDR}}$ is the penalty factor of the heat load change subsidy coefficient; α_1 and α_2 are the boundaries of the heat load change, respectively.

Similarly, the subsidy coefficient when the cold load changes can also be expressed as follows:

$$\varepsilon_{c,\mathrm{IDR}} = \begin{cases} \varepsilon_{c,\mathrm{IDR}}, & 0 < \left|\Delta L_c(t)\right| < \beta_1, \\ \left(1+\lambda_{c,\mathrm{IDR}}\right)\varepsilon_{c,\mathrm{IDR}}, & \beta_1 \le \left|\Delta L_c(t)\right| \le \beta_2, \\ \left(1+2\lambda_{c,\mathrm{IDR}}\right)\varepsilon_{c,\mathrm{IDR}}, & \left|\Delta L_c(t)\right| > \beta_2, \end{cases} \tag{41}$$

where $\lambda_{c,\mathrm{IDR}}$ is the penalty factor of the cold load change subsidy coefficient and β_1 and β_2 are the dividing boundaries of the cold load change respectively.

4.3. Substitution-Type IDR Model. Since heat and cold loads are slower dynamic than electric and gas loads, this article only considers the substitution between heat and cold loads and the substitution between electric and gas loads and establishes the heat and cold substitution IDR and the electric substitution IDR model, respectively.

4.3.1. Heat and Cold Substitution IDR Model. Since there are a variety of energy conversion devices inside the IES, the same energy needs of users can be met through mutual conversion of heat and cold energy. The heat and cold replacement IDR model can be expressed as follows:

$$\begin{cases} \Delta L_{c,\mathrm{AL}}^t = -\varepsilon_{h-c}\Delta L_{h,\mathrm{AL}}^t, \\ \varepsilon_{h-c} = \dfrac{W_h\eta_h}{W_c\eta_c}, \end{cases} \tag{42}$$

where $\Delta L_{h,\mathrm{AL}}^t$ and $\Delta L_{c,\mathrm{AL}}^t$ are the response quantity of heat and cold load replacement; W_h and W_c are the unit calorific values of heat and cold load; ε_{h-c} is the heat-cold conversion absorption; and η_h and η_c are the utilization efficiency of heat and cold energy.

4.3.2. Electric Substitution IDR Model. Based on the real-time price difference between electricity and gas, users can choose an energy with lower cost to replace another energy. For example, during peak electricity price periods, users can increase gas energy input to replace electricity consumption if gas prices are relatively low. The electric substitution IDR model can be expressed as follows:

$$\begin{cases} \Delta L_{e,\mathrm{AL}}^t = \varepsilon_{e-g}\dfrac{c_e^t - c_g^t}{c_g^t}L_{e,\mathrm{AL},0}^t, \\ \Delta L_{g,\mathrm{AL}}^t = -\lambda_{e-g}\Delta L_{e,\mathrm{AL}}^t, \end{cases} \tag{43}$$

where $\Delta L_{e,\mathrm{AL}}^t$, $\Delta L_{g,\mathrm{AL}}^t$ are the amounts of electric and gas loads replacement response; ε_{e-g} is the elastic coefficient of electricity and gas affected by price; $L_{e,\mathrm{AL},0}^t$ is the amount of electric load that can be replaced before response; and λ_{e-g} is the electricity-gas conversion efficiency.

5. IES Optimization Model

5.1. Objective Function. The model proposed in this paper comprehensively considers energy purchase cost F_{Buy}, reward and punishment ladder-type carbon transaction cost F_{CET}, green certificate transaction mechanism F_{GCT}, and operation and maintenance cost F_{OM} and IDR subsidy cost F_{IDR} to optimize the IES model with the goal of minimizing the total cost where F_{CET} and F_{GCT} are shown in formulas (30) and (31) and formula (16), respectively. The objective function of IES can be expressed as follows:

$$\min\ F_{\mathrm{IES}} = F_{\mathrm{Buy}} + F_{\mathrm{OM}} + F_{\mathrm{CET}} + F_{\mathrm{IDR}} + F_{\mathrm{GCT}}. \tag{44}$$

5.1.1. Energy Purchase Cost. The energy purchase cost of IES includes electricity purchase cost and gas purchase cost, which can be expressed as follows:

$$\begin{aligned} &F_{\mathrm{Buy}} = F_{\mathrm{Grid},b} + F_{\mathrm{Gas},b}, \\ &\begin{cases} F_{\mathrm{Grid},b} = \sum_{t=1}^{T} c_e(t)P_{\mathrm{Grid}}(t), \\ F_{\mathrm{Gas},b} = \sum_{t=1}^{T} c_g(t)\left(\dfrac{P_{\mathrm{CHP},g}(t) + P_{\mathrm{GB},g}(t)}{H_{\mathrm{ng}}}\right), \end{cases} \end{aligned} \tag{45}$$

where $F_{\mathrm{Grid},b}$ and $F_{\mathrm{Gas},b}$ are the electricity purchase cost and gas purchase cost of IES, respectively; $c_e(t)$ is the outsourced electricity price purchased by IES from the external power grid; $c_g(t)$ is the gas purchase price of IES; H_{ng} is the lower calorific value of natural gas; and $P_{\mathrm{CHP},g}(t)$ and $P_{\mathrm{GB},g}(t)$ are the amount of natural gas consumed by CHP and GB, respectively.

5.1.2. Operation and Maintenance Cost.

$$F_{\mathrm{OM}} = \left(\sum_{t=1}^{T}\sum_{n}\varepsilon_n P_n(t) + \sum_{m}\kappa_m\left(P_{m,\mathrm{chr}}(t) + P_{m,\mathrm{dis}}(t)\right)\right), \tag{46}$$

where n represents the type of energy conversion equipment; m represents the type of energy storage equipment; ε_n and κ_m are the operation and maintenance coefficients of energy conversion equipment n and energy storage equipment m, respectively; $P_n(t)$ is the output power of energy conversion equipment n; and $P_{m,\mathrm{chr}}(t)$ and $P_{m,\mathrm{dis}}(t)$ are the charging

and discharging power of the energy storage device m, respectively.

5.1.3. Incentive-Type IDR Subsidy Costs.

$$F_{\mathrm{IDR}} = \sum_{t=1}^{T} \left(E_{e,\mathrm{IDR}}(t) + E_{h,\mathrm{IDR}}(t) + E_{c,\mathrm{IDR}}(t) + E_{g,\mathrm{IDR}}(t) \right). \tag{47}$$

5.2. Constraints. In addition to meeting the upper and lower limit constraints and ramp rate constraints of each device, IES also needs to meet the power balance constraints.

5.2.1. Power Balance Constraint. Power balance constraint is as follows:

$$P_{\mathrm{WT}}(t) + P_{\mathrm{PV}}(t) + P_{\mathrm{CHP},e}(t) + P_{\mathrm{Grid}}(t) + P_{\mathrm{BT,dis}}(t) + P_{\mathrm{HFC},e}(t) = L_e(t) + P_{\mathrm{BT,chr}}(t) + P_{\mathrm{EL},e}(t) + P_{\mathrm{AC},e}(t). \tag{48}$$

5.2.2. Heat Energy Balance Constraint. Heat energy balance constraint is as follows:

$$P_{\mathrm{GB}}(t) + P_{\mathrm{CHP},h}(t) + P_{\mathrm{HST,dis}}(t) + P_{\mathrm{HFC},h}(t) = L_h(t) + P_{\mathrm{HST,chr}}(t) + P_{\mathrm{AR},h}(t). \tag{49}$$

5.2.3. Cold Energy Balance Constraint. Cold energy balance constraint is as follows:

$$P_{\mathrm{AC},c}(t) + P_{\mathrm{AR},c}(t) + P_{\mathrm{CST,dis}}(t) = L_c(t) + P_{\mathrm{CST,chr}}(t). \tag{50}$$

5.2.4. Natural Gas Energy Balance Constraint. Natural gas energy balance constraint is as follows:

$$P_{\mathrm{Gas}}(t) + P_{\mathrm{GST,dis}}(t) = L_g(t) + P_{\mathrm{CHP},g}(t) + P_{\mathrm{GB},g}(t) - P_{\mathrm{MR},g}(t) + P_{\mathrm{GST,chr}}(t), \tag{51}$$

where $P_{\mathrm{Gas}}(t)$ is the amount of natural gas purchased.

5.2.5. Hydrogen Energy Balance Constraint. Hydrogen energy balance constraint is as follows:

$$P^t_{\mathrm{EL},H_2} = P^t_{\mathrm{MR},H_2} + P^t_{\mathrm{HFC},H_2} + P^t_{\mathrm{HES,dis}} - P^t_{\mathrm{HES,chr}}. \tag{52}$$

6. Case Analysis

6.1. Basic Data. In order to verify the effectiveness of the IES optimal scheduling proposed in this paper, a simulation example is carried out with a park-level CCHP IES as the object. The park is dominated by residents, supplemented by industry and commerce. The time-of-use prices of electricity and gas are shown in Table 2 [8, 12], the power curves of user electricity, heat, cold, and gas loads as well as photovoltaic power and wind power are shown in Figures 4 and 5 [12, 31, 32], and the internal equipment parameters of IES are shown in Table 3 [8, 12, 32]. In terms of IDR parameters [12–14, 31], the upper and lower limits of indoor temperature are 24°C and 18°C, respectively; the subsidy coefficients for electric and gas loads are 0.05 and 0.04, respectively, and the subsidy coefficients for heat and cold loads are both 0.03. The upper limit of the rate is 10%; the penalty factor of the subsidy coefficient for heat and cold load changes is 0.01. The unit carbon transaction price is 0.268 yuan/kg [8, 29], the green certificate transaction price is 80 yuan/book [26, 30], and μ and λ are 0.2 and 0.15, respectively; the actual carbon emission parameters of coal-fired units and gas-fired units can be seen in Table 4 [8]. The model proposed in this article is constructed under the platform of MATLAB, and the mathematical model and constraints of IES are formed on the basis of Yalmip toolbox. The CPLEX commercial solver is used to do the calculation.

6.2. Validation of Hydrogen Energy Utilization Model. In order to highlight the effectiveness of the hydrogen energy coupling system in improving system economy and environmental protection, the following five scenarios are set up for comparative analysis. The comparison results of the five scenarios are shown in Table 5.

Scenario 1. The traditional electricity-heat/cold-gas IES scheduling model is introduced, without considering the multisource energy storage equipment

Scenario 2. Based on scenario 1, multisource energy storage equipment is introduced

Scenario 3. Based on scenario 2, EL, MR, and HES are introduced, and hydrogen only for MR

Scenario 4. Based on scenario 3, HFC is introduced, and hydrogen for MR and HFC

Scenario 5. Based on scenario 4, the gas-hydrogen mixed CHP equipment, i.e., the hydrogen energy multiutilization model proposed in this article, is considered

6.2.1. Comparative Analysis of Scenario 1 and Scenario 2. The comparison between scenario 1 and scenario 2 is conducted first. The power balance optimization results of scenario 1 and scenario 2 are shown in Figures 6 and 7, respectively. After calculation, it can be seen from Table 5 that compared with scenario 1, the total IES cost and carbon emissions of scenario 2 decreased by 2.81% and 3.38%, respectively. Since scenario 1 does not introduce multi-energy storage equipment, IES cannot absorb abundant renewable energy when the energy load is at a low point, resulting in low energy utilization efficiency. During the peak load period, energy cannot be discharged through the energy storage device, resulting in a greater pressure on the energy supply of the IES during the peak load period, resulting in higher energy purchases for the system during the peak period of electricity consumption, resulting in more electricity purchase costs.

Table 2: Time-of-use prices of electricity and gas.

Initial electricity price	Time period	Yuan/kWh/m^3
Valley	1:00–6:00, 23:00-24:00	0.5
Level	7:00-8:00, 13:00–17:00	0.73
Peak	9:00–12:00, 18:00–22:00	1.21
Initial gas price	Time period	Yuan·m^{-3}
Valley	23:00-24:00, 01:00–05:00	1.57
Level	6:00-7:00, 13:00–16:00, 19:00–22:00	1.93
Peak	8:00–12:00, 17:00-18:00	2.16

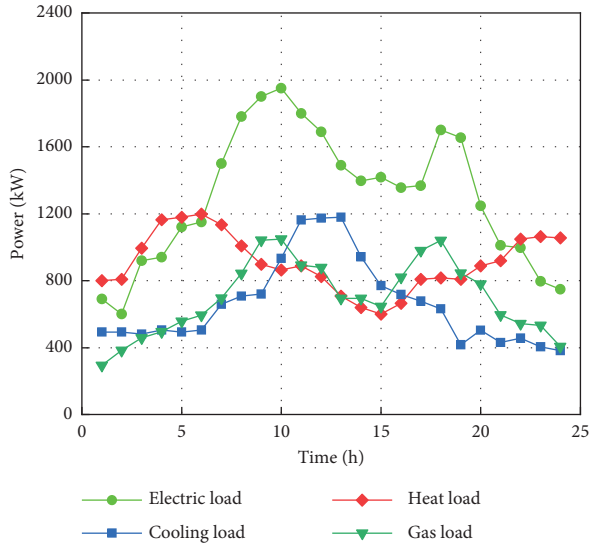

Figure 4: Forecast curve of electricity, heat, cold, and gas.

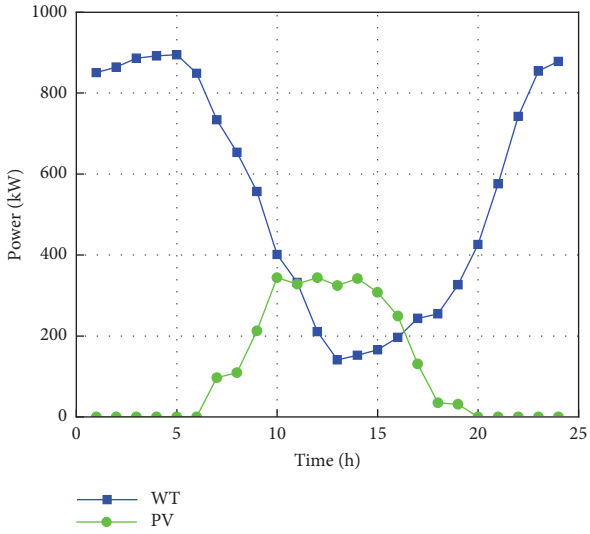

Figure 5: Forecast curve of wind turbine and photovoltaic power.

As shown in Figure 6(b) in the heat energy scheduling of scenario 1, the gas-fired boiler is basically at full power during the period of high heat load from 01:00 to 05:00. The shortage can only be supplemented by the waste heat boiler, due to the limitation of "determining electricity by heat" of CHP devices, so the gas turbine must also contribute, resulting in the inability to absorb wind power resources at night, which makes the operating cost of the IES higher. As for scenario 2, it can be seen from Figure 7 that the four energy storage devices of electricity, heat, cold, and gas can all store energy at the stage of low energy load and discharge energy at the period of high energy load, which plays a role in low-charging. As for the effect of high radiation, combined with Table 5, it can be seen that when multiple energy storage devices are introduced, the operating economy of IES has been greatly improved.

6.2.2. Comparative Analysis of Scenario 2 and Scenario 3. Then, the comparison between scenario 2 and scenario 3 is performed. In scenario 3, a hydrogen energy coupling link consisting of EL, HES, and MR is introduced, but the HFC and hydrogen-mixed CHP models are not considered. The balance results of electricity, heat, gas, and cold scheduling in scenario 3 are shown in Figure 8. It can be seen from Figure 8 that after the hydrogen energy coupling consisting of EL, HES, and MR, the abundant wind power resources at night can be input into the EL to generate hydrogen energy. However, since it only contains one hydrogen energy utilization link (MR) and consumes one more cascade utilization link compared with the traditional P2G model, its energy utilization efficiency is relatively low. As can be seen from Table 4, compared with scenario 2, the total IES cost and carbon emissions of scenario 3 increased by 0.77% and 0.63%, respectively.

Table 3: IES equipment parameters.

Energy conversion equipment	Efficiency	Rated power (kW)	Ramp power (kW)
CHP	Electricity 0.45, heat 0.55	900	200
GB	0.9	1200	200
EL	0.87	400	100
HFC	0.95	250	50
MR	0.7	200	50
ER	1.2	500	—
AC	4	150	—
Energy storage device	Charge/discharge efficiency	Maximum capacity (kW)	Maximum charging/discharging power (kW)
BT	0.95	1000	250
HST	0.97	1000	200
CST	0.92	800	200
GST	0.90	800	200
HES	0.95	600	150

Table 4: IES actual carbon emission parameters.

Coal-fired unit			Gas-fired unit		
x_1	y_1	z_1	x_2	y_2	z_2
36	−0.38	0.0034	3	−0.004	0.001

6.2.3. Comparative Analysis of Scenario 2 and Scenario 4. On the basis of scenario 3, scenario 4 further introduces HFC equipment. The power balance scheduling results of electricity, heat, cold, and gas in scenario 4 are presented in Figure 9. It can be seen from the calculation in Table 4 that compared with scenario 2 and scenario 3, the total cost of IES in scenario 4 dropped by 1.69% and 2.45%, respectively, and the carbon emissions dropped by 5.92% and 6.51%, respectively. For scenario 4, there are more ways to utilize hydrogen energy after the introduction of HFC. The hydrogen generated through EL can be directly transported to HFC for heat and electricity production, which can provide users with electricity and heat energy to cover the shortage and reduce the energy supply pressure of the system. In addition, the hydrogen generated by EL can also be transported to MR and CHP to generate the electricity, heat, and gas energy, which can be supplied to user loads respectively. Through the above steps, abundant wind power resources can be effectively utilized to achieve multi-energy coupling of electricity-heat-cold-gas-hydrogen.

6.2.4. Comparative Analysis of Scenario 4 and Scenario 5. Compared with scenario 4, scenario 5 constructs a hydrogen-doped CHP system by introducing a hydrogen-doping device into the CHP unit. It further increases the ways of utilizing the hydrogen energy and forms a multiple utilization of hydrogen energy. Part of the hydrogen energy can be input into the natural gas pipeline and then be input into the hydrogen-doped CHP at the same time as the natural gas for thermoelectric production, further improving the flexibility of IES operation. As can be seen from Table 4, compared with scenario 4, the total cost of IES and system carbon emissions in scenario 5 decreased by 0.78% and 1.98%, respectively, which proves that with the continuous improvement of the hydrogen energy utilization structure, the operational flexibility and economy of IES will be better.

6.3. Validation of Multitype Demand Response. In order to verify the effectiveness of the multitype IDR strategy proposed in this paper, on the basis of scenario 3, three new scenarios are added for comparison.

Scenario 6. Only the price-type IDR strategy is considered

Scenario 7. The price-type and incentive-type IDR strategies are considered

Scenario 8. The multitype IDR strategy proposed in this paper is considered; the comparative results of the four scenarios are shown in Table 6.

It can be seen from Table 6 that among the four scenarios, scenario 5 has the highest total IES cost and carbon emissions. Since the IDR strategy is not considered in scenario 3, the user cannot adjust the energy load independently, which will cause the IES to bear higher energy purchase costs during the period of high energy load, making the operating cost increase. Besides, compared with other scenarios, the carbon emissions of scenario 3 are relatively high due to the lack of load transfer or reduction. For scenarios 6–8, the more types of IDRs considered, the smaller the total cost and carbon emissions of IES. The reason is that users are more willing to participate in IDR with the increase of IDR types. Although the incentive-type IDR will increase the cost of incentive subsidies, the operating cost of the IES is reduced due to the reduction of part of the energy load. Correspondingly, as the energy load decreases, the output of IES equipment decreases, which indirectly reduces the carbon emissions of the system. It can be seen from Table 6 that compared with scenario 6 and scenario 7, the total cost of IES in scenario 8 with multitype IDR strategy decreased by 11.63%, 8.43%, and 6.25%, respectively, and the total carbon emissions decreased by 18.82%, 9.63%, and 6.94%, respectively. All the data indicates the effectiveness of multitype IDR strategy.

The optimization results of real-time prices of electricity and gas are shown in Figure 10, and the optimization results of electricity, gas, heat, and cold loads in four scenarios are represented in Figure 11. Since scenario 5 does not consider the IDR strategy, there is no load change. In scenario 6, as can be seen from Figure 10, under the action of real-time

Table 5: Cost comparison results under different scenarios.

Scenes	IES total cost (yuan)	Operation and maintenance cost (yuan)	Energy purchase cost (yuan)	Carbon emission (kg)
1	33408.9	4741.3	28667.6	17809.1
2	32466.8	4500.9	27965.9	17206.5
3	32716.4	4701.3	28015.6	17314.5
4	31915.3	4824.5	27090.8	16187.4
5	31666.4	4870.1	26796.3	15867.2

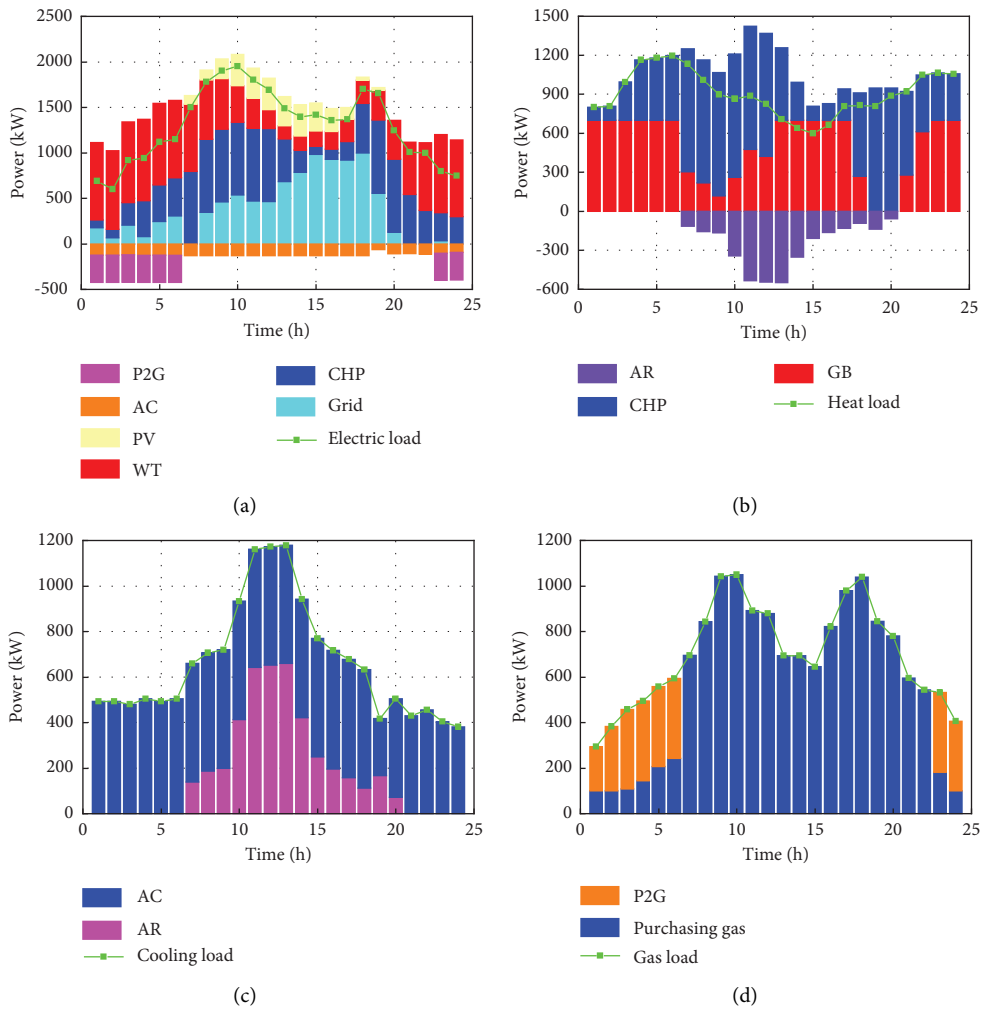

Figure 6: (a) Electricity scheduling results in scenario 1; (b) heat scheduling results in scenario 1; (c) cold energy scheduling results in scenario 1; (d) gas energy scheduling results in scenario 1.

price IDR, the optimized peak-valley-level trend of electricity and gas prices is consistent with the corresponding benchmark price trend, but the change range is greater. In general, the price during peak periods is higher and lower during valley periods. Thus, the peak-valley-level difference in energy prices further increases. Combining the red curves in Figures 11(a) and 11(b), it can be seen that under the guidance of real-time prices, the electricity and gas loads transfer the load from the peak energy consumption period to the low energy consumption period, realizing the effect of load "peak shaving and valley filling." Since the real-time price IDR strategy only considers electricity and gas loads, the heat and cold loads do not change.

On the basis of scenario 6, scenario 7 further introduces an incentive-type IDR strategy. The user's electricity and gas loads can be partially reduced according to the incentive strategy, while the cold and heat loads can be reasonably adjusted within the comfort range based on changes in indoor temperature, water temperature, and various external heat disturbance factors. Incentive subsidies are provided for certain adjustment of user's electric and gas loads. Figure 11(d) shows the change of cold load with indoor

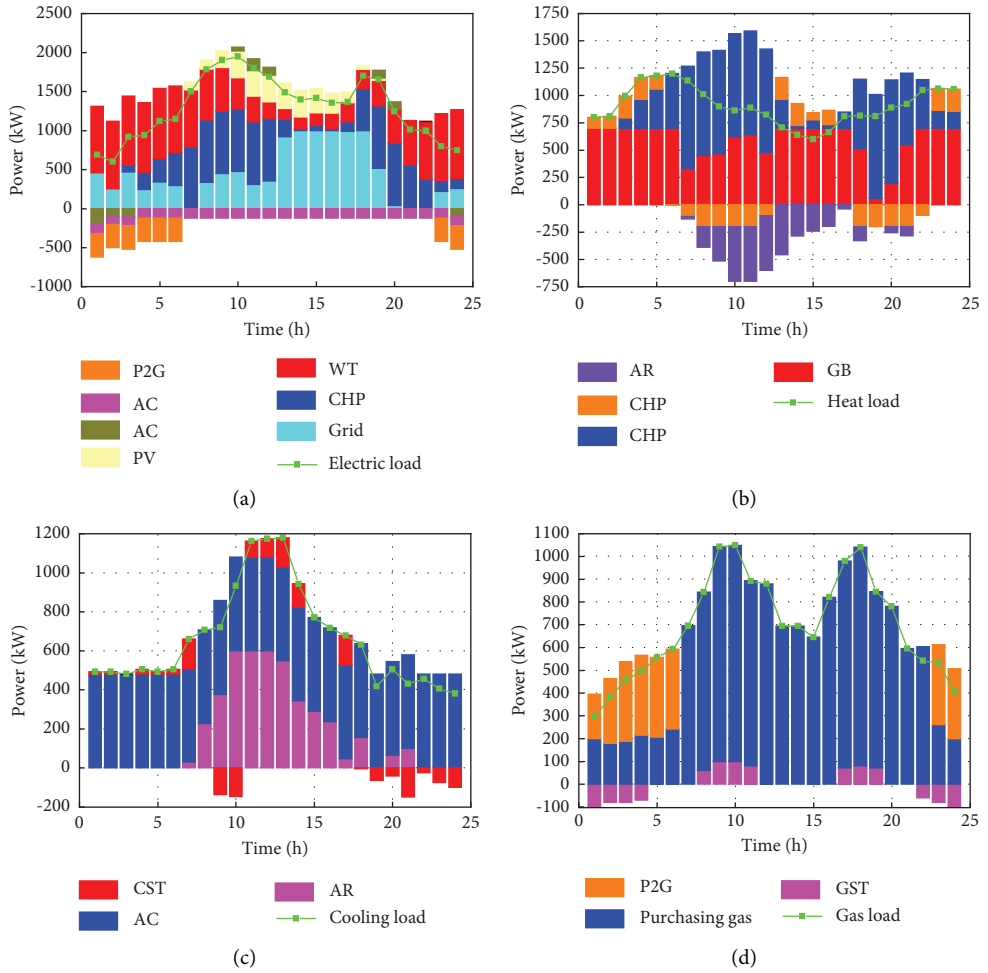

Figure 7: (a) Electricity scheduling results in scenario 2; (b) heat scheduling results in scenario 2; (c) cold energy scheduling results in scenario 2; (d) gas energy scheduling results in scenario 2.

temperature. It can be seen that IES stores a certain amount of heat by lowering the indoor temperature during the period of low cold load from 01:00 to 06:00 at night, which increases the cold load in this period, while IES releases stored heat by raising the indoor temperature to reduce the cold load during the day when the cold load is high, which can reduce the electricity cost of the refrigeration equipment and improve the system economy. The optimization results for heat load are similar as above. As can be seen from Figure 11, the peak and valley differences in electricity, heat, cold, and gas loads in scenario 7 have been further reduced.

For scenario 8, price-type IDR, incentive-type IDR, and substitution-type IDR strategies are comprehensively considered. Since the energy costs of various energy sources vary greatly at different times, users can improve the economics of the system through energy substitution to reduce their own energy purchase costs. It can be seen from the real-time price optimization results in Figure 9 that users choose electric energy instead of gas energy during the period of 23:00–06:00 for the lower electricity price, increasing the electric load. And users are more inclined to choose gas energy instead of electric energy during the peak electricity price periods such as 9:00–12:00 and 18:00–21:00, decreasing the electric load. The peak shaving and valley filling trend of electric load has further increased in Figure 11. In the same way, the substitution optimization trend of cold and heat loads is similar to the above. However, the energy peak-valley characteristics of cold and heat loads are exactly opposite, which means that the peak period of heat load happens to be the valley period of cold load. As a result, the cold and heat loads also appear the effect of peak shaving and valley filling. It can be seen from Table 6 that the total cost of IES and total carbon emissions in scenario 8 have been effectively reduced, indicating that alternative IDR can provide users with diversified energy purchasing options without affecting the user's energy experience. It improves the economy and flexibility of the system and also effectively reduces the carbon emissions of the system.

6.4. Validation of Green Certificate-Carbon Joint Trading Mechanism. In order to verify the environmental protection and economics of the green certificate-reward and

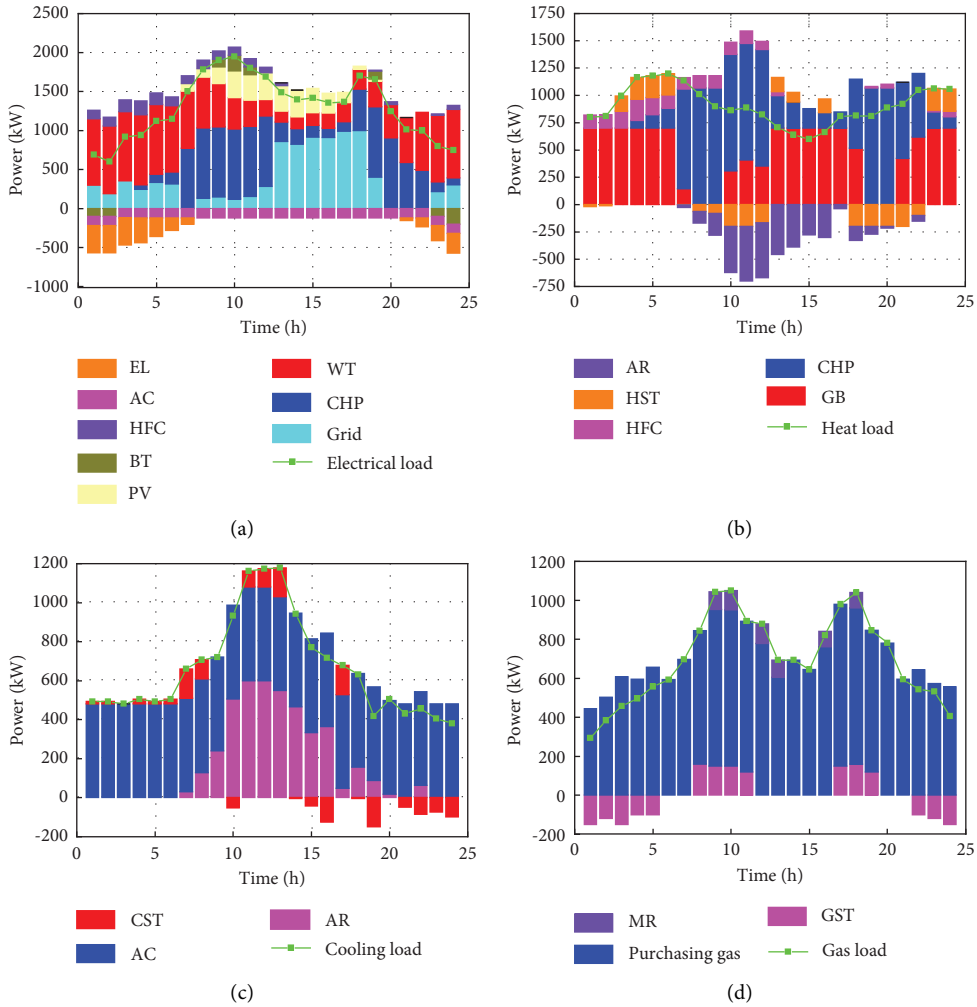

Figure 8: (a) Electricity scheduling results in scenario 3; (b) heat scheduling results in scenario 3; (c) cold energy scheduling results in scenario 3; (d) gas energy scheduling results in scenario 3.

punishment ladder-type carbon trading mechanism proposed in this paper in improving the optimization operation of hydrogen energy coupling IES, four new scenarios are added for comparative analysis with scenario 8.

Scenario 9. Hydrogen coupled IES optimization model considering the green certificate trading mechanism

Scenario 10. Hydrogen coupled IES optimization model considering the reward and punishment ladder-type carbon trading mechanism.

Scenario 11. Hydrogen coupled IES optimization model considering the green certificate trading mechanism and the reward and punishment ladder-type carbon trading mechanism, but without considering the joint mechanism of the two

Scenario 12. Scenario of this article, hydrogen coupled IES optimization model considering green certificate-ladder carbon joint trading

6.4.1. Comparative Analysis of Scenario 9 and Scenario 8. Scenario 9 is an optimization scenario that only considers the green certificate transaction mechanism. It can be seen from Table 7 that the carbon emissions of the system and the total cost of IES in scenario 6 decreased by 2.22% and 1.65% compared with scenario 8, respectively. After introducing the green certificate trading mechanism, scenario 9 has abundant green certificate due to the large proportion of green power (wind power and photovoltaic), which can be traded in the market. It not only improves the consumption capacity of renewable energy such as photovoltaic and photovoltaic but also receives a certain amount of income from green certificate transactions, which verifies the effectiveness of the green certificate transaction mechanism.

6.4.2. Comparative Analysis of Scenario 10 and Scenario 8. Scenario 10 introduces traditional carbon trading costs into the IES optimization model based on scenario 8. The comparison results of outsourced electricity and CHP in scenario 8 and scenario 10 are shown in Figure 12. Table 6

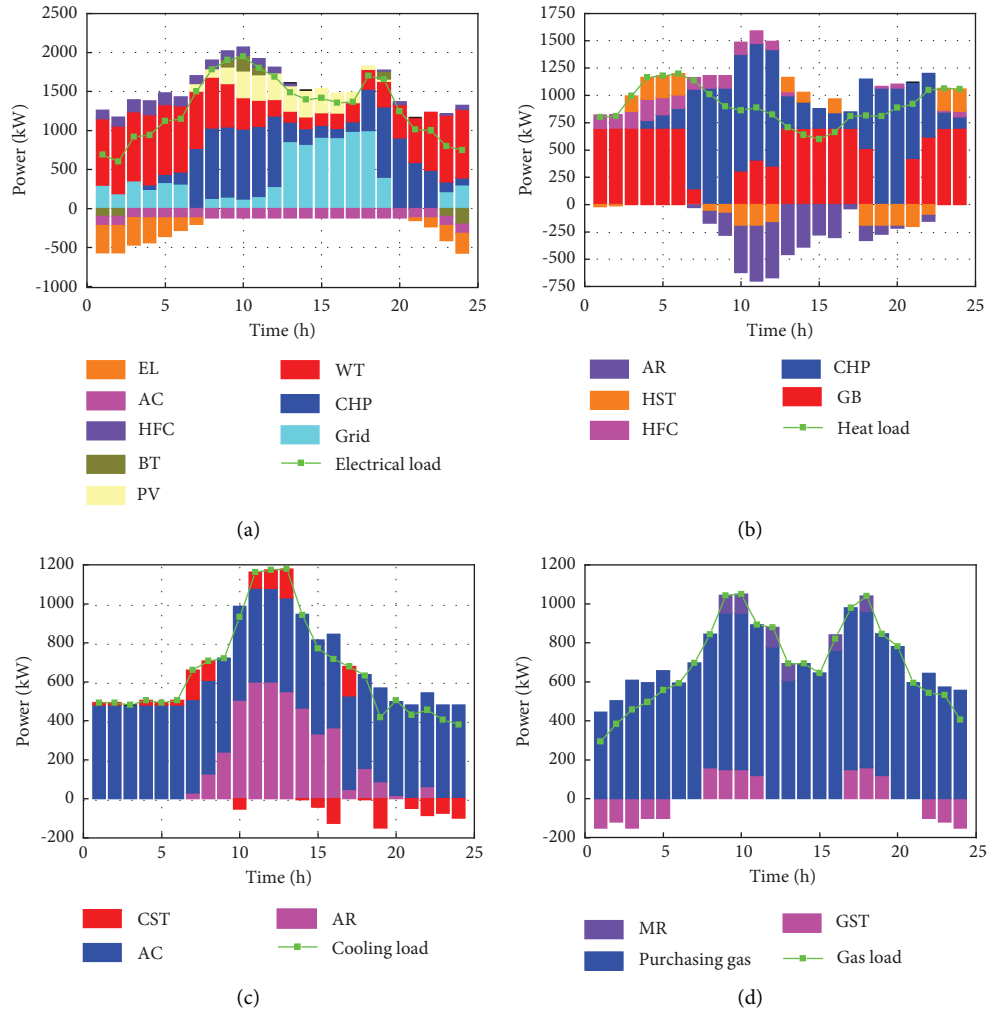

Figure 9: (a) Electricity scheduling results in scenario 4; (b) heat scheduling results in scenario 4; (c) cold energy scheduling results in scenario 4; (d) gas energy l scheduling results in scenario 4.

Table 6: Comparison of scheduling costs under different IDR strategies.

Scenes	IES total cost (yuan)	Operation and maintenance cost (yuan)	Energy purchase cost (yuan)	IDR subsidy cost (yuan)	Carbon emission (kg)
5	31666.4	4870.1	26796.3	—	15867.2
6	30416.4	4802.5	25613.9	—	14120.2
7	29567.1	4715.4	23843.6	1008.1	13841.4
8	27981.7	4971.4	21885.8	1124.5	12880.4

shows that the total cost of IES and carbon emissions of the system in scenario 10 decreased by 1.67% and 10.55% compared with scenario 8. The specific reason is that scenario 8 does not introduce reward and punishment ladder-type carbon trading costs into the IES optimization model, so IES only optimizes the optimal output of the unit with the goal of optimizing its own interests. It can be seen from Figure 12 that the amount of outsourced electricity from the external grid is much bigger during the valley or level period of electricity price between 23:00–06:00 and 13:00–18:00 due to its lower costs than the electricity generated by gas turbines thus resulting in a large amount of carbon emissions. As for scenario 10, the carbon transaction costs are introduced into the optimization model, and IES can sell the excess carbon allowances in the carbon trading market due to the large output of gas-fired units in the IES to obtain certain carbon trading benefits. By choosing the output power of gas units with lower carbon emissions, such as CHP and GB, the total carbon emissions of the system can be effectively reduced.

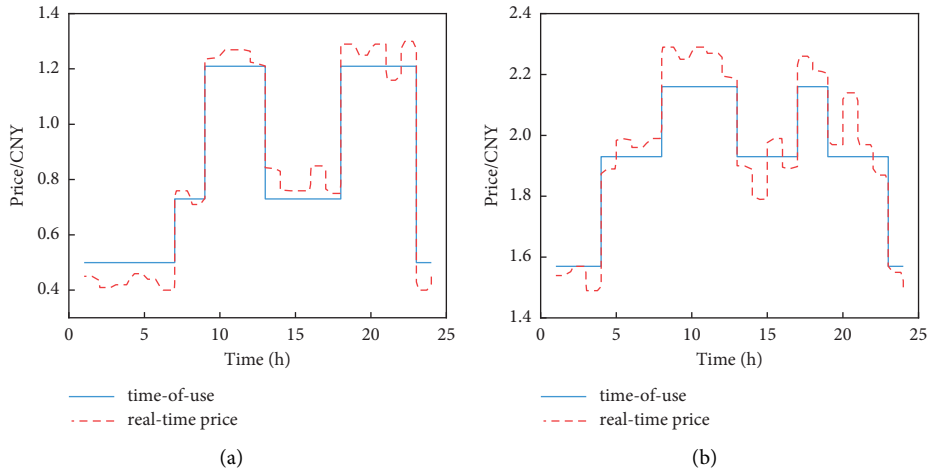

Figure 10: Optimization results of real-time electricity price and time-of-use electricity price. (a) Electricity price optimization results. (b) Gas price optimization results.

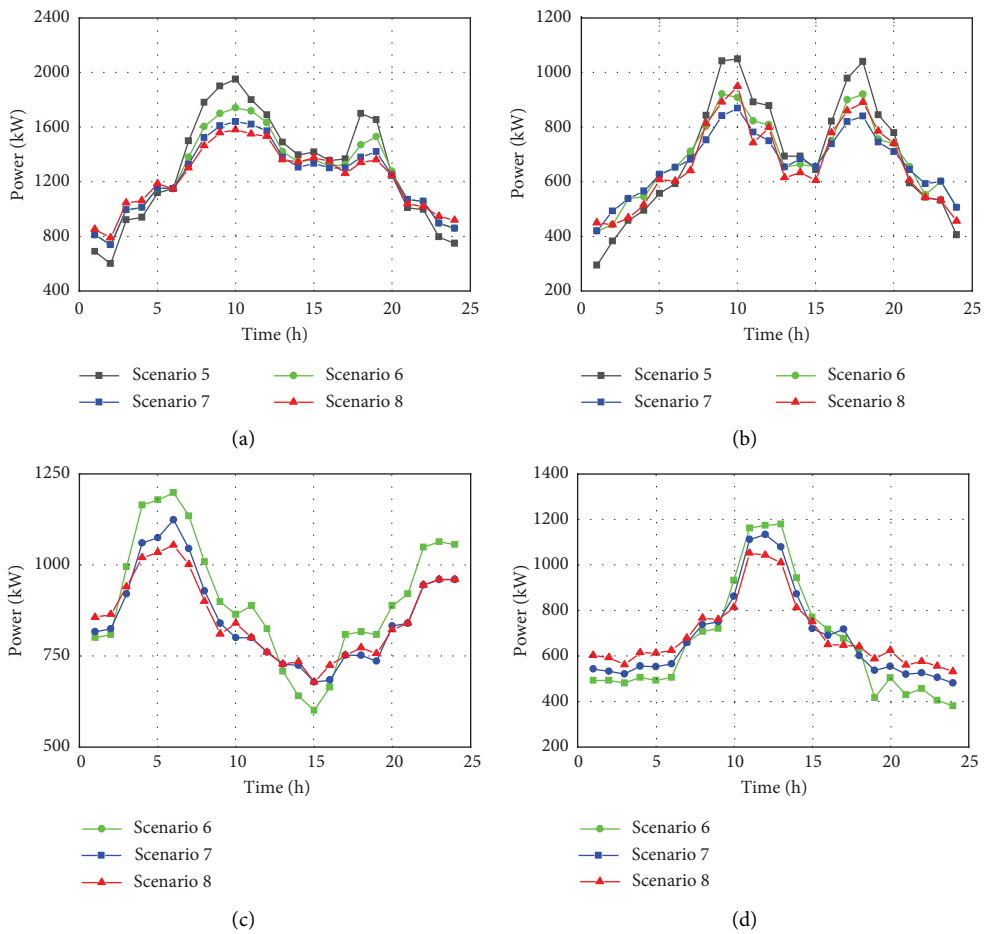

Figure 11: Optimization results of electricity, heat, cold, and gas loads. (a) Electrical load optimization results. (b) Gas load optimization results. (c) Heat load optimization results. (d) Cooling load optimization results.

6.4.3. Analysis on the Effectiveness of the Green Certificate-Carbon Joint Trading Mechanism. For scenario 11, the reward and punishment ladder-type carbon trading mechanism and the green certificate trading mechanism are simultaneously used in the hydrogen energy coupling IES optimal scheduling. As can be seen from Table 7, compared with the other three schemes, the IES in scenario 11 reduces the carbon trading cost, obtains certain benefit from the

Table 7: Comparative results of different scheduling schemes.

Scenario	IES total cost (yuan)	Operation and maintenance cost (yuan)	Energy purchase cost (yuan)	IDR subsidy cost (yuan)	Carbon trading cost (yuan)	Green certificate trading cost (yuan)	Carbon emission
8	28443.4	4981.7	22403.6	1058.1	—	—	12690.8
9	26924.2	4884.8	22118.4	1340.1	—	−1419.1	11709.4
10	27514.1	4901.9	22082.0	1078.1	−547.9	—	11520.4
11	26415.8	4942.1	22219.7	1211.5	−558.1	−1399.4	11048.4
12 (this article)	25989.1	4911.3	22071.7	1240.3	−815.1	−1419.1	10751.6

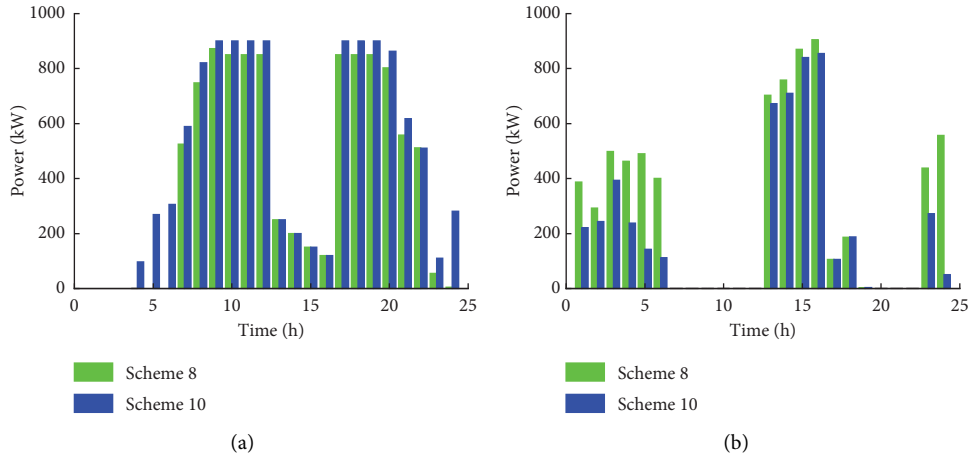

FIGURE 12: Comparison of outsourced electricity and gas turbine output under different schemes. (a) Output power of CHP. (b) Purchased electricity.

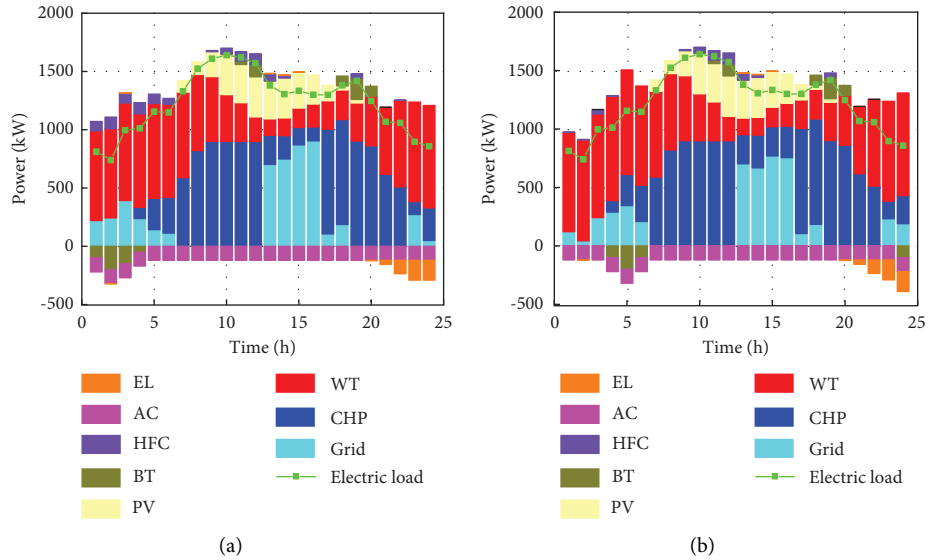

FIGURE 13: Electricity scheduling results (a) for scenario 11 and (b) for scenario 12.

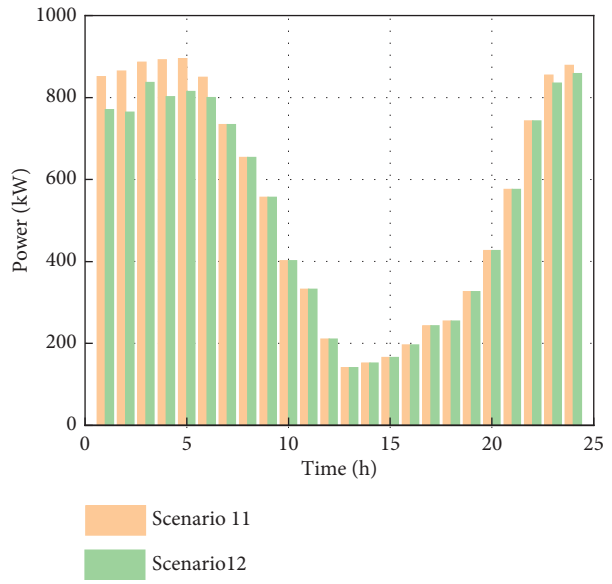

FIGURE 14: Comparative results of wind power consumption in scenario 11 and scenario 12.

green certificate trading, and minimizes the total cost and carbon emissions. On the basis of scenario 11, scenario 12 further considers the interaction between the green certificate trading mechanism and carbon trading. The reduction of carbon emissions provided by new energy can affect the carbon trading mechanism, decrease the amount of carbon emissions of IES, and increase the enthusiasm of IES to purchase green certificates, indicating the low-carbon economy of the green certificate-carbon joint trading strategy. Figures 13 and 14 show the power scheduling results and wind power consumption comparison results of scenarios 11 and 12 respectively. It can be seen from Figures 13 and 14 that scenario 12 has a higher wind power consumption level at night such as 01:00, 06:00, and 24:00 than scenario 11. In addition, the gas unit output in scenario 12 is higher, and the outsourced power is smaller, reflecting the low-carbon nature of the green certificate-carbon joint trading. As can be seen from Table 7, the total IES cost and carbon emissions of scenario 12 decreased by 1.61% and 2.68% compared with scenario 11, which verifies the effectiveness of the green certificate-carbon joint trading mechanism proposed in this article.

7. Conclusion

This paper proposes a hydrogen energy coupling IES optimization operation model that takes into account the green certificate-ladder carbon joint trading mechanism and integrated demand response. The effectiveness of the multiple utilization of hydrogen energy, dual-incentive demand response, and green certificate-ladder carbon joint trading mechanism can be verified through the simulation example. The following conclusions can be obtained:

(1) By introducing a multiutilization model of hydrogen energy composed of EL, HFC, MR, and hydrogen-mixed CHP, the surplus wind power at night is converted into hydrogen energy, and hydrogen energy is converted into electricity, heat, and gas energy through various links. It effectively improves the consumption capacity of new energy and reduces energy purchase costs and carbon emissions of the system. Compared with the traditional electricity-heat-gas IES, the total cost and carbon emissions of this IES decreased by 2.46% and 7.78% after introducing the multiple utilization model of hydrogen energy, which reflects the effectiveness of the proposed multiple utilization model of hydrogen energy.

(2) A dual-incentive IDR model consisting of price incentives and subsidy incentives is constructed, and users are guided to adjust their own energy consumption strategies through price strategies and subsidy incentives, respectively. It not only reduces the energy purchase cost of users but also effectively reduces the operating costs and carbon emissions of the system. Compared with the traditional price-type demand response model, the total cost and carbon emissions of IES decreased by 10.17% and 25.27% after considering the dual-incentive IDR model. It verifies the effectiveness of multiple dual-incentive IDR models in improving the economy and environmental protection of IES.

(3) Introducing the green certificate trading mechanism and the ladder carbon trading mechanism into the IES optimization model can give full play to the complementarity of the two mechanisms and further enhance the low-carbon characteristics of the system. Compared with only considering the GCT mechanism or CET mechanism, the total cost of IES decreased by 3.47% and 5.54%, and the carbon emissions decreased by 8.18% and 6.67%, respectively, after considering the green certificate-carbon joint trading mechanism.

Data Availability

The data used to support the findings of this study are available from the corresponding author upon request.

Conflicts of Interest

The authors declare that there are no conflicts of interest regarding the publication of this paper.

Acknowledgments

This work was supported by the Key Technology Research Project for the High Quality Development of the "Land Scenery Three Gorges" in Jilin Province-Park Level Multi Microgrid System Participation in Grid Friendly Interaction (Project no. 202303003SF).

References

[1] H. Chang, Z. Wan, Y. Zheng et al., "Energy analysis of a hybrid PEMFC–solar energy residential micro-CCHP system combined with an organic Rankine cycle and vapor compression cycle," *Energy Conversion and Management*, vol. 142, pp. 374–384, 2017.

[2] L. Wang, C. Hou, B. Ye, X. Wang, C. Yin, and H. Cong, "Optimal operation analysis of integrated community energy system considering the uncertainty of demand response," *IEEE Transactions on Power Systems*, vol. 36, no. 4, pp. 3681–3691, 2021.

[3] S. Xie, Z. Hu, J. Wang, and Y. Chen, "The optimal planning of smart multi-energy systems incorporating transportation, natural gas and active distribution networks," *Applied Energy*, vol. 269, Article ID 115006, 2020.

[4] H. Li, Z. Wei, Q. Miao, L. Zhao, B. Sun, and C. Zhang, "Multi-energy flow cooperative dispatch for generation, storage, and demand in integrated energy systems with dynamic correction," *Sustainable Cities and Society*, vol. 76, 2021.

[5] S. Xu, H. Zhang, X. Lin, Z. Li, and Z. Chen, "Optimal day-ahead dispatching strategy for polymorphic energy self-consistent system with supply and demand for offshore island," *Zhongguo Dianji Gongcheng Xuebao/Proceedings of the Chinese Society of Electrical Engineering*, vol. 39, 2019.

[6] T. Yuan, G. Li, Z. Zhang, L. Zhang, and S. Mei, "Optimal modeling on equipment investment planning of wind power-hydrogen energy storage and coal chemical pluripotent

coupling system," *Transactions of China Electrotechnical Society*, vol. 31, 2016.

[7] L. Zhu, J. Wang, L. Tang, S. Liu, and C. Huang, "Robust stochastic optimal dispatching of integrated energy systems considering refined power-to-gas model," *Power System Technology*, vol. 43, 2019.

[8] J. Chen, Z. Hu, Y. Chen, and W. Chen, "Thermoelectric optimization of integrated energy system considering ladder-type carbon trading mechanism and electric hydrogen production," *Dianli Zidonghua Shebei/Electric Power Automation Equipment*, vol. 41, no. 9, 2021.

[9] A. Karapetyan, M. Khonji, C. K. Chau, K. Elbassioni, H. Zeineldin, and T. H. M. El-Fouly, "A competitive scheduling algorithm for online demand response in islanded microgrids," *IEEE Transactions on Power Systems*, vol. 36, no. 4, 2021.

[10] J. Wang, H. Zhong, Z. Ma, Q. Xia, and C. Kang, "Review and prospect of integrated demand response in the multi-energy system," *Applied Energy*, vol. 202, pp. 772–782, 2017.

[11] Z. Guo, G. Li, M. Zhou, and W. Feng, "Resilient configuration approach of integrated community energy system considering integrated demand response under uncertainty," *IEEE Access*, vol. 7, pp. 87513–87533, 2019.

[12] T. Zhang, Y. Guo, Y. Li, and J. Zhang, "Optimization scheduling of regional integrated energy systems based on electric-thermal-gas integrated demand response," *Dianli Xitong Baohu yu Kongzhi/Power System Protection and Control*, vol. 49, no. 1, 2021.

[13] S. Zheng, Y. Sun, B. Li, B. Qi, X. Zhang, and F. Li, "Incentive-based integrated demand response for multiple energy carriers under complex uncertainties and double coupling effects," *Applied Energy*, vol. 283, Article ID 116254, 2021.

[14] M. A. Mirzaei, A. Sadeghi Yazdankhah, and B. Mohammadi-Ivatloo, "Stochastic security-constrained operation of wind and hydrogen energy storage systems integrated with price-based demand response," *International Journal of Hydrogen Energy*, vol. 44, no. 27, pp. 14217–14227, 2019.

[15] Y. Wang, Y. Wang, Y. Huang et al., "Planning and operation method of the regional integrated energy system considering economy and environment," *Energy*, vol. 171, pp. 731–750, 2019.

[16] Y. Wang, Y. Wang, Y. Huang et al., "Operation optimization of regional integrated energy system based on the modeling of electricity-thermal-natural gas network," *Applied Energy*, vol. 251, Article ID 113410, 2019.

[17] J. Qiu, Z. Y. Dong, J. H. Zhao, K. Meng, Y. H. Zheng, and D. J. Hill, "Low carbon oriented expansion planning of integrated gas and power systems," *IEEE Transactions on Power Systems*, vol. 30, no. 2, pp. 1035–1046, 2015.

[18] Y. Cui, P. Zeng, W. Zhong, W. Cui, and Y. Zhao, "Low-carbon economic dispatch of electricity-gas-heat integrated energy system based on ladder-type carbon trading," *Dianli Zidonghua Shebei/Electric Power Automation Equipment*, vol. 41, no. 3, 2021.

[19] L. Wang, H. Dong, J. Lin, and M. Zeng, "Multi-objective optimal scheduling model with igdt method of integrated energy system considering ladder-type carbon trading mechanism," *International Journal of Electrical Power and Energy Systems*, vol. 143, Article ID 108386, 2022.

[20] M. Wu, J. Xu, Y. Li et al., "Low carbon economic dispatch of integrated energy systems considering life cycle assessment and risk cost," *International Journal of Electrical Power and Energy Systems*, vol. 153, Article ID 109287, 2023.

[21] C. Chen, X. Shen, T. Xia, Q. Guo, H. Sun, and Y. Chen, "Multi-objective optimal dispatch method for integrated energy system considering exergy efficiency," *Dianli Xitong Zidonghua/Automation of Electric Power Systems*, vol. 43, no. 12, 2019.

[22] J. Yang, N. Zhang, Y. Cheng, C. Kang, and Q. Xia, "Modeling the operation mechanism of combined p2g and gas-fired plant with co 2 recycling," *IEEE Transactions on Smart Grid*, vol. 10, no. 1, pp. 1111–1121, 2019.

[23] Y. Ma, H. Wang, F. Hong et al., "Modeling and optimization of combined heat and power with power-to-gas and carbon capture system in integrated energy system," *Energy*, vol. 236, no. 5, Article ID 121392, 2021.

[24] Q. Peng, X. Zhou, and R. Yang, "Design of coordination and balance mechanism between national green power certificate trading market and provincial day-ahead power market," *Dianwang Jishu/Power System Technology*, vol. 44, no. 7, 2020.

[25] Y. Fu, Z. Wei, K. Xu, and L. Pang, *Investigation On The Comprehensive Energy Conservation Management For Urban And Rural Distribution*, Environmental Science Engineering, 2012.

[26] H. Mehrjerdi, H. Saboori, and S. Jadid, "Power-to-gas utilization in optimal sizing of hybrid power, water, and hydrogen microgrids with energy and gas storage," *Journal of Energy Storage*, vol. 45, Article ID 103745, 2022.

[27] Q. Ting, L. Huaidong, W. Jinqiao, F. Zhiqiang, F. Wei, and T. University, "Carbon trading based low-carbon economic dispatch for integrated electricity-heat-gas energy system," *Automation of Electric Power Systems*, vol. 42, 2018.

[28] S. Cheng, R. Wang, J. Xu, and Z. Wei, "Multi-time scale coordinated optimization of an energy hub in the integrated energy system with multi-type energy storage systems," *Sustainable Energy Technologies and Assessments*, vol. 47, no. 22, Article ID 101327, 2021.

[29] J. Jin, P. Zhou, C. Li, X. Guo, and M. Zhang, "Low-carbon power dispatch with wind power based on carbon trading mechanism," *Energy*, vol. 170, pp. 250–260, 2019.

[30] X. Ji, M. Li, M. Li, and H. Han, "Low-carbon optimal operation of the integrated energy system considering integrated demand response," *Frontiers in Energy Research*, vol. 11, Article ID 1283429, 2023.

[31] G. De, X. Wang, X. Tian, T. Xu, and Z. Tan, "A collaborative optimization model for integrated energy system considering multi-load demand response," *Energies*, vol. 15, no. 6, p. 2033, 2022.

[32] H. Zhang, Y. Chen, K. Liu, and S. Dehan, "A novel power system scheduling based on hydrogen-based micro energy hub," *Energy*, vol. 251, Article ID 123623, 2022.